Microbial production of the low-caloric sweetener D-allulose from D-glucose by evolutionary engineering

Alexander Lehnert[1], Rocco Gentile[3], Claudia Tahiraj[1], Astrid Wirtz[1], Meike Baumgart[1], Tino Polen[1], Holger Gohlke[2,3,4], Michael Bott[1,4*]

[1]IBG-1: Biotechnology, Institute of Bio- and Geosciences, Forschungszentrum Jülich, Jülich, Germany

[2]IBG-4: Bioinformatics, Institute of Bio-and Geosciences, Forschungszentrum Jülich, Jülich, Germany

[3]Insitute for Pharmaceutical and Medicinal Chemistry, Heinrich-Heine-Universität Düsseldorf, Düsseldorf, Germany

[4]The Bioeconomy Science Center (BioSC), Forschungszentrum Jülich, Jülich, Germany

[*]Corresponding author: m.bott@fz-juelich.de

Abstract

The low-calorie sugar D-allulose is a promising alternative to D-sucrose and high-fructose corn syrup, but its microbial production from D-glucose at mesophilic temperatures is limited by insufficient D-glucose isomerase (XylA) activity. Here, we overcome this bottleneck by evolving a *Corynebacterium glutamicum* selection strain whose growth strictly depends on XylA function. This strategy yielded a XylA variant with a nine-fold higher catalytic efficiency, sugar transporter variants (IolT1) with ten-fold increased activity for D-glucose and D-fructose, and hints for co-transport of these sugars by the D-sucrose transporter PtsS. Molecular dynamics simulations provided possible mechanistic explanations for the adaptive mutations. Combining the evolved enzymes with a suitable D-allulose 3-epimerase in a highly engineered chassis strain enabled whole-cell conversion of D-glucose to D-allulose with a 15% yield at 30 °C. This performance rivals immobilized enzyme processes performed at ~60°C while avoiding enzyme purification and immobilization, offering an alternative for low-calorie sweetener production.

Keywords: *Corynebacterium glutamicum*, adaptive laboratory evolution, molecular dynamics simulations, sugar uptake, alternative sweetener, D-fructose, D-glucose, D-allulose

Introduction

The overconsumption of food and beverages sweetened with high-caloric D-sucrose or high-fructose corn syrup (HFCS) causes numerous health problems, such as obesity, type 2 diabetes, and cardiovascular diseases [1,2]. In order to reduce the consumption of D-sucrose and HFCS, numerous low-caloric sweeteners have been introduced, such as saccharine, aspartame, xylitol, or stevioside, several of which have undesired traits [3]. D-Allulose, also named D-psicose, is a rare natural sugar, the C3 epimer of D-fructose, that gained strong interest as a dietary sweetener, as it

41 has 70% of the sweetness of D-sucrose, but less than 10% of its caloric content (≤0.4 kcal/g) [4].
42 In 2024, the global D-allulose market was valued at approximately USD 148 million and was
43 projected to grow at a compound annual growth rate (CAGR) of 14% from 2025 to 2034, expected
44 to reach around USD 553 million by 2034 by Global Market Insights Inc. D-Allulose is generally
45 recognized as safe by the FDA (GRAS Notice 400) and its consumption is associated with positive
46 health effects, such as attenuation of blood glucose levels and reduction of body weight [5,6].

47 The industrial production of D-allulose is performed in enzyme reactors, either from D-
48 fructose via a one-step conversion with D-allulose 3-epimerase or D-tagatose 3-epimerase, or from
49 D-glucose in a two-step conversion including additionally a D-glucose isomerase (XylA) [7]. D-
50 Glucose isomerase is in fact a D-xylose isomerase having the physiological function to convert D-
51 xylose to D-xylulose, which after phosphorylation can be metabolized in the pentose phosphate
52 pathway. As a side-reaction this enzyme also catalyzes the conversion of D-glucose to D-fructose
53 and therefore is also called D-glucose isomerase, which is the term generally used in this study [8].
54 D-Glucose isomerases are used in the industrial production of HFCS, which is a mixture of D-
55 glucose and D-fructose that is used as a sweetener for beverages and processed foods at a >10
56 million tons scale per year. HFCS is produced at 60-70°C to compensate for the poor activity of
57 D-glucose isomerases towards D-glucose at mesophilic temperatures and to shift the
58 thermodynamic equilibrium of the isomerization towards D-fructose [9]. D-Glucose isomerase
59 research therefore focused on the isolation of more active and thermostable variants either by
60 protein engineering or by using isoenzymes from hyperthermophilic microorganisms [10-12]. In
61 contrast, no studies have been reported aiming at identifying D-glucose isomerases with improved
62 activity at mesophilic temperatures. In the current industrial D-allulose production from D-glucose,
63 the use of high temperatures of ≥50°C for the efficient isomerization of D-glucose to D-fructose
64 poses a challenge, since D-allulose 3-epimerases or D-tagatose 3-epimerases generally reveal a low

65 stability at this temperature range [13]. Hence, immobilization of the enzymes is used to increase
66 their stability and reusability. Combined with immobilized D-glucose isomerases, the production
67 of D-allulose from D-glucose via isomerization and epimerization achieves yields of 10-16% [14-
68 16].

69 In this study, we engineered bacterial strains that efficiently produce D-allulose from D-
70 glucose at 30°C via D-glucose isomerase and D-allulose 3-epimerase for applications in the food
71 and beverage industry. Such an approach avoids the necessity of protein purification, protein
72 immobilization, and high operating temperatures (≥50°C), thereby reducing energy and material
73 demands while improving product stability. The major bottleneck was to enable a fast conversion
74 of D-glucose to D-fructose within the cells by D-glucose isomerase. To solve this problem, we
75 employed adaptive laboratory evolution (ALE). As host we chose *Corynebacterium glutamicum*,
76 an industrially well established microbe that is used since decades for amino acid production in the
77 million ton scale and whose products are generally regarded as safe (GRAS) [17,18]. Of particular
78 importance in the context of our study was the previous detailed knowledge on sugar uptake and
79 metabolism in *C. glutamicum* [19]. D-Glucose, D-fructose, and D-sucrose are taken up via
80 phosphoenolpyruvate-dependent phosphotransferase systems (PTS) with the EII transporters PtsG,
81 PtsF, and PtsS that form D-glucose 6-phosphate, D-fructose 1-phosphate, and D-sucrose 6-
82 phosphate, respectively. A small fraction of D-fructose is imported by PtsG forming D-fructose 6-
83 phosphate [20]. D-Sucrose 6-phosphate is converted by D-sucrose 6-phosphate hydrolase to D-
84 glucose 6-phosphate and D-fructose [21]. As *C. glutamicum* lacks fructokinase activity, the
85 imported D-fructose cannot be metabolized and is exported by an unknown transporter followed
86 by reimport via PtsF and PtsG [20]. Besides PTS transport, uptake of certain sugars can also be
87 catalyzed by the H^+-coupled secondary transporters IolT1 and IolT2. Their native substrates are
88 inositols [22,23], but due to their promiscuity, they can also transport D-fructose [24] and D-

89 glucose [25,26]. In contrast to D-fructose, imported D-glucose can be metabolized by *C.*
90 *glutamicum* after phosphorylation to D-glucose 6-phosphate by the endogenous glucokinases Glk
91 and PpgK [27,28]. Based on this knowledge, we engineered a selection strain whose growth was
92 strictly dependent on the isomerization of D-fructose to D-glucose by the provided D-glucose
93 isomerase. In a few rounds of ALE, fast-growing clones were obtained and found to harbor
94 mutations in only two targets, XylA and IolT1, causing increased D-glucose isomerase activity and
95 an increased activity for D-fructose uptake into the cytoplasm. The combination of the evolved
96 XylA and IolT1 proteins in a chassis strain unable to grow on D-glucose, D-fructose, and D-sucrose
97 and equipped with a D-allulose 3-epimerase enabled the conversion of D-glucose to D-allulose at
98 30°C with yields of about 15% that are comparable to the industrial processes using immobilized
99 enzymes at >50°C.
100
101 **Results**
102 **Growth-based selection for high *in vivo* D-glucose isomerase activity at 30°C**
103 D-Glucose isomerases have a very low affinity for D-glucose, with K_m values typically above
104 100 mM (Table S1 in the supplemental information online). Whereas in processes with
105 immobilized D-glucose isomerases much higher D-glucose concentrations can be provided to
106 enable high enzyme activity, the D-glucose concentration within microbial cells is usually much
107 lower, as D-glucose is immediately metabolized in the central metabolism. In order to obtain
108 microbial strains enabling a high conversion rate of D-glucose to D-fructose within the cells, we
109 used ALE with a selection strain of *C. glutamicum* whose growth at 30°C was strictly dependent
110 on the isomerization of D-fructose to D-glucose. As first step, the genes for the EII permeases PtsG
111 and PtsF were deleted to prevent uptake of D-glucose and D-fructose as D-glucose 6-phosphate
112 and D-fructose 1-phosphate, respectively, as these metabolites cannot serve as substrates for the

113 D-glucose isomerase. To enable the import of unphosphorylated D-glucose and D-fructose,
114 expression of the *iolT1* gene was made constitutive by relieving its repression by its native
115 transcriptional regulator IolR [29] via promoter mutations [30]. Growth of the resulting Fru^{neg}
116 strain (Figure 1A) was tested in a BioLector microcultivation system, which measures the cell
117 density online as backscatter signal [31]. The strain showed negligible growth in D-fructose
118 minimal medium, while growth in D-glucose minimal medium was only slightly reduced ($\mu = 0.34$
119 $\pm 0.02\ h^{-1}$) compared to the parental strain MB001 ($\mu = 0.45 \pm 0.01\ h^{-1}$) due to the lack of PtsG
120 (Figure 1B-C). Based on these results, *C. glutamicum* Fru^{neg} was a suitable seletion strain for the
121 isolation of improved D-glucose isomerase variants.

122 Seven genes for D-glucose isomerases that were previously reported to show activity for D-
123 glucose or D-xylose at 30°C (Table S1 in the supplemental information online) were cloned into
124 plasmid pPREx2 under the control of an IPTG-inducible *tac* promoter and transferred into strain
125 Fru^{neg} (Figure 1A). The resulting strains were then tested for growth on D-fructose in the BioLector.
126 To observe small growth differences, inoculation was performed to a high optical density at 600 nm
127 (OD_{600}) of 7.5. The final OD_{600} of the cultures was measured spectrophotometrically and D-
128 fructose titers in the culture supernatant were determined via HPLC. All seven selected D-glucose
129 isomerases improved growth of the Fru^{neg} strain (Figure 1D, Figure S1 in the supplemtal
130 information online), but differed with respect to the growth rate and D-fructose consumption
131 (Figure 1E). The enzymes of *Anoxybacillus gonensis* ($XylA_{AG}$), *Arthrobacter* strain N.R.R.L.
132 B3728 ($XylA_{AB}$) and *Xanthomonas campestris* ($XylA_{XC}$) enabled the highest growth rates in D-
133 fructose minimal medium, but only $XylA_{AB}$ and $XylA_{XC}$ also resulted in a high D-fructose
134 consumption by the Fru^{neg} strain, supporting a direct link between growth and D-fructose
135 isomerization. Hence, $XylA_{AB}$ and $XylA_{XC}$ were selected for the ALE experiments.

136

137 **Adaptive laboratory evolution of the Fru^{neg} strain carrying *xylA* expression plasmids**

138 XylA$_{AB}$ and XylA$_{XC}$ slightly improved growth of the Fru^{neg} strain in D-fructose minimal medium,
139 but both corresponding strains barely doubled their initial OD_{600} and consumed less than 20% of
140 the provided D-fructose during 160 h of cultivation, confirming severe bottlenecks in the
141 conversion of D-fructose to D-glucose. To eliminate these bottlenecks, the strains Fru^{neg} pPREx2-
142 *xylA*$_{AB}$ (AB) and Fru^{neg} pPREx2-*xylA*$_{XC}$ (XC) were subjected to laboratory evolution by selecting
143 for faster growth. The ALE experiment was performed with three biological replicates of each
144 strain in 24-well plates (Figure 2A). After 3-5 serial cultivations in D-fructose minimal medium
145 lasting for 5-15 days each over a total period of 45-55 days, the growth rate and the cell density of
146 all six cultures were strongly increased. Then, aliquots of each culture were plated at a 1:100,000
147 dilution on D-fructose minimal medium agar plates. Small and large colonies appeared after 4-5
148 days of incubation at 30°C and one single large colony of each plate was picked and used for a
149 growth experiment in the BioLector. All six evolved clones (called FAB evo 1-3 and FXC evo 1-
150 3) grew much faster and reached a much higher OD_{600} than the parental and control strains and
151 consumed the entire D-fructose, showing that evolution was successful (Figure 2B-C, Figure S2A-
152 B in the supplemental information online).

153 To elucidate the molecular basis for the improved growth of the evolved strains, first their
154 plasmids were sequenced (Table 1). In pPREx2-*xylA*$_{AB}$ of strain FAB evo 1 a mutation causing a
155 S2F exchange in XylA was identified, whereas strains FAB evo 2 and FAB evo 3 both harbored a
156 cytosine to thymine exchange 20 bp upstream of the *xylA*$_{AB}$ start codon in pPREx2-*xylA*$_{AB}$ (6 bp
157 upstream of the ribosome binding site). The latter mutation might cause improved translation of
158 the *xylA* mRNA leading to more XylA protein and higher enzyme activity. The XylA$_{AB}$-S2F
159 mutation might also enable an increased translation of the *xylA* mRNA. Remarkably, the plasmids
160 of the three independently evolved strains with the *X. campestris xylA* gene all carried an identical

161 mutation leading to a W147S exchange in $XylA_{XC}$. We assume that this single mutation increases
162 the enzymatic activity for D-fructose isomerization to D-glucose. Next the genomic DNA of the
163 six evolved strains was sequenced. Interestingly, all genomes were found to carry only a single
164 mutation which was located in the *iolT1* gene (Table 1). Four strains (FAB evo 1, FAB evo 3, FXC
165 evo 1, and FXC evo 2) contained a G87S exchange in IolT1, whereas two strains (FAB evo 2 and
166 FXC evo 3) harbored a T351P exchange in IolT1. The results suggested that the combination of
167 two effects was responsible for enabling improved growth on D-fructose, namely an improved
168 activity of D-glucose isomerase for D-fructose conversion to D-glucose and an improved D-
169 fructose uptake to increase the cytoplasmic D-fructose concentration and thereby XylA activity.
170

171 **Reverse engineering to confirm the relevance of the ALE-derived mutations**

172 To confirm the relevance of the individual mutations and the assumption that a combination of
173 *xylA* and *iolT1* mutations is required to achieve fast growth on D-fructose, we performed reverse
174 engineering and introduced the mutations singly or in combination into the parent Fru^{neg} strain
175 carrying either pPREx2-$xylA_{AB}$ or pPREx2-$xylA_{XC}$. In total, 18 strains carrying either the single
176 mutations *iolT1*-T351P, *iolT1*-G87S, $xylA_{AB}$-S2F, $xylA_{AB}$(c_t), and $xylA_{XC}$-W147S or various
177 combinations were constructed by homologous recombination, checked for correctness, and tested
178 for growth in D-fructose minimal medium. As shown in Figure 2D-G and Figure S2C-F in the
179 supplemental information online, all introduced mutations showed a positive effect on growth, but
180 the mutations in *iolT1*, i.e. T351P and G87S, stimulated growth and D-fructose consumption more
181 strongly than the different *xylA* mutations. While pPREx2-*xylA* related mutations increased the
182 growth rate maximally twofold, the G87S or T351P mutations in *iolT1* enhanced the growth rate
183 by three- to sevenfold. However, the combination of *iolT1* and *xylA* mutations was necessary and

184 sufficient to obtain strains with growth characteristics similar to the ALE strains containing the
185 same mutations.
186
187 **Effect of the IolT1 mutations on the kinetics of D-fructose and D-glucose transport**
188 The effects of the amino acid exchanges G87S and T351P found in IolT1 were analyzed by
189 determining the growth rate of the Fru^{neg} strain with either wild-type IolT1, IolT1-G87S
190 ($IolT1^{G87S}$), IolT1-T351P ($IolT1^{T351P}$), or IolT1-G87S-T351P ($IolT1^{G87S-T351P}$) at varying
191 concentrations of D-fructose. The concentration enabling the half-maximal growth rate represents
192 the K_s value. For this experiment, the strains were transformed with plasmid pPREx2-*scrK* that
193 encodes a fructokinase from *Clostridium acetobutylicum* known to be active in *C. glutamicum*
194 [32,33]. With this enzyme, D-fructose taken up by IolT1 is phosphorylated to D-fructose 6-
195 phosphate enabling growth of the cells in D-fructose minimal medium [20] independent of D-
196 glucose isomerase activity.
197 Strain Fru^{neg} pPREx2-*scrK* with wild-type IolT1 grew poorly in D-fructose minimal medium
198 with a maximal growth rate (μ_{max}) of 0.032 ± 0.002 h^{-1} and a K_S value of 106.9 ± 7.6 mM (Figure 3,
199 Figure S3 in the supplemental information online, Table 2). The strains with the variants $IolT1^{G87S}$,
200 $IolT1^{T351P}$, and $IolT1^{G87S-T351P}$ showed an about 10-fold increased growth rate with K_S values
201 reduced by 10-32% (Table 2). These results confirmed that both mutations found in IolT1 after
202 ALE strongly improve its ability for D-fructose transport. A combination of both mutations
203 improved μ_{max} slightly, but concomitantly increased the K_S value. Hence, the double mutation did
204 not show an additive effect and the two single mutations are sufficient to boost D-fructose uptake.
205 Besides D-fructose, we also tested the growth rate dependency on the D-glucose concentration.
206 In this case, no plasmid was required due to the availability of the endogenous glucokinases Glk
207 and PpgK [27,28]. Compared to D-fructose, the Fru^{neg} strain with wild-type IolT1 reached an

208 almost ten-times higher μ_{max} of 0.296 ± 0.010 h^{-1} and a six-times lower K_S value of 18.9 ± 2.8 mM
209 (Figure 3, Figure S3 in the supplemental information online, Table 2), revealing a clear preference
210 of IolT1 for D-glucose over D-fructose. The strains with the variants IolT1^{G87S}, IolT1^{T351P}, and
211 IolT1$^{G87S-T351P}$ almost doubled their μ_{max} values, while revealing strongly reduced K_S values by
212 factors of 4 - 14 (Table 2). As in the case of D-fructose, the combined mutations did not improve
213 D-glucose transport. In summary, these experiments confirmed that the amino acid exchanges
214 G87S and T351P in IolT1 have a strongly positive effect on D-fructose and D-glucose transport,
215 presumably leading to increased cytoplasmic concentrations of these sugars, thereby stimulating
216 their conversion by D-glucose isomerase.
217
218 **Molecular dynamics simulations of the IolT1 variants**
219 To assess the influence of the G87S and T351P substitutions on the structural stability of IolT1,
220 we performed all-atom unbiased MD simulations of structural models of IolT1 in four different
221 configurations (outward-open, outward-occluded, inward-occluded, inward-open), in part bound
222 to D-glucose (as β-D-glucopyranose, BGP) and D-fructose (as β-D-fructofuranose, BFF), inserted
223 into the lipid bilayer according to the OPM (Orientations of Proteins in Membranes) database
224 (Figure S4-10 and Table S2 in the supplemental information online) [34]. Starting structures of the
225 IolT1 variants were generated using the FoldX suite [35]. In all cases, the change in the folding
226 free energy $\Delta\Delta G$ upon the G87S and T351 substitutions is <3 kcal/mol, indicating that they are not
227 considered destabilizing [36]. The membrane composition used was phosphatidylglycerol 16:0-
228 18:1, cardiolipin 16:0-18.1, and phosphatidylinositol 16:0-18:1 in a ratio of 6:2:1, resembling the
229 composition of the inner membrane of *C. glutamicum* [37]. For each configuration, five replicas
230 were simulated, each for 2.0 μs in length, of which the last 1.5 μs were used for analysis. We used
231 the generated conformations to probe if substitutions G87S, T351P, and G87S-T351P change the

232 structural stability of IolT1 by applying a model of dynamic allostery [38,39] previously used on
233 receptors and transporters [40,41]. The model describes allosteric effects due to substitutions in
234 terms of the per-residue (i, eq. 2, Supplemental Methods) or per-region (r, eq. 3, Supplemental
235 Methods) rigidity index $\Delta r_{i/r,(Mutant - WT)}$ [39]. We evaluated $\Delta r_{i/r,(Mutant - WT)}$ for the helices 290-306
236 and 390-401, which are involved in the binding of the carbohydrate ligand in the outward-occluded
237 and inward-occluded configurations and are critical for the carbohydrate transport to the inside of
238 the cell, as found for the human GLUT transporter [42]. There, the helices are named TM7b and
239 TM10b. Conformational changes of these helices during the transport cycle are common in the
240 major facilitator superfamily (MFS) [43] and accompany the rocker-switch mechanism used by
241 MFS transporters.

242 The helices 290-306 and 390-401 of IolT1 are more than 20 Å and 12 Å away from the
243 substitutions G87S and T351P, respectively (Figure 4A). The substitutions are also not located near
244 other parts of the transport route, so that a trivial effect on the transport process is unlikely. The
245 model of dynamic allostery revealed a configuration-, substitution type-, and carbohydrate-
246 dependent impact of the amino acid substitutions on the structural stability of both helices 290-306
247 and 390-401. First, the substitutions destabilize the helices in the outward-open configuration,
248 whereas they stabilize them in the inward-open configuration (Figure 4A-B). In between, in the
249 outward-occluded configuration, helix 290-306 becomes destabilized and helix 390-401 stabilized;
250 in turn, in the inward-occluded configuration, helix 290-306 is stabilized and helix 390-401 is
251 destabilized. In either case, the destabilization or stabilization is less than in the outward-open or
252 inward-open configurations, respectively. Second, these effects decrease in the order of the
253 substitutions T351P > G87S > G87S-T351P, i.e., in correlation with the substitution effects on the
254 growth rate (Figure 3). Note that substitution effects on structural stability are not necessarily
255 additive, which can explain why the impact of the double substitution is lower than that of the

256 single ones [44]. Finally, the (de-)stabilizing effects for the two occluded states are generally
257 weaker in the case of bound D-fructose than D-glucose (Figure 4B), again in line with the
258 difference in growth rates between the two carbohydrates (Figure 3). Compared to wild-type IolT1,
259 this leads to a succession of configurations with increasing structural stability along the transport
260 cycle (Figure 4B), which favors the inward-open configuration as the most structurally stable.
261 These changes could result in the enhanced transport of the cargo from the outside to the inside of
262 the cell.

263 While the gradient-driven transport is initiated by the binding of the cargo to the outward-open
264 configuration [45], the reset of the transporter from the inward-open to the outward-open
265 configuration is known for other carbohydrate transporters, such as the lactose permease of *E. coli*
266 [46,47], to involve interactions of lipid head groups with charged amino acids to accommodate the
267 energetic barrier imposed by salt bridges in the inward-open configuration. In IolT1, after the
268 release of the carbohydrate on the intracellular side, D46 in TM1 and E400 in TM10b are thought
269 to trigger the resetting between inward- and outward-facing conformations similarly to what has
270 been suggested in other carbohydrate transporters [46,47]. MD simulations of IolT1 revealed that
271 the PG lipid headgroups interact with D46 and E400, which form salt bridges to R126 (100.0% of
272 total frames) and R339 (75.9% of total frames), respectively (Figure S11-12 in the supplemental
273 information online). The substitutions do not affect such salt bridges (Figure S11-12 in the
274 supplemental information online), thus, they should not influence the reset process.

275 To explain the difference in transport between D-glucose and D-fructose, we assessed the
276 impact of helices 290-306 and 390-401 on carbohydrate binding in the outward-occluded and
277 inward-occluded states by computing residue-wise effective binding energies. D-Glucose was
278 found to bind stronger than D-fructose, in both the wild-type protein and the variants, and
279 irrespective of the IolT1 configuration (Figure 4C). A less favorable binding of D-fructose likely

280 impacts the transport rate of the carbohydrate. The IolT1 variants revealed stronger interactions
281 with the carbohydrates than wild-type IolT1, suggesting that allosteric effects due to the
282 substitutions can improve the binding of the carbohydrates in addition to impacting the structural
283 stability of the transporter (Figure 4C). To conclude, substitutions T351P and G87S allosterically
284 impact functionally relevant helices of IolT1, and the impacts correlate with the increase of the
285 growth rates enabled by these substitutions.
286
287 **Effects of mutations in XylA on its kinetic properties**
288 ALE-mediated selection for faster growth on D-fructose resulted in three different mutations with
289 respect to the *xylA* gene, i.e. $xylA_{AB}$-S2F, $xylA_{AB}$(c_t), and $xylA_{XC}$-W147S (Table 1). Mutations in
290 the 5'-untranslated region (5'-UTR) and at the second codon of $xylA_{AB}$ can influence gene
291 expression levels, e.g. by stabilization of the mRNA or enhancing translation initiation [48-50]. To
292 test the effect of the S2F and c_t mutations on the XylA protein level, Western blot analysis was
293 performed. Both mutations led to a much higher protein content compared to wild-type $XylA_{AB}$
294 (Figure S13A in the supplemental information online), suggesting that the improved growth of
295 strains carrying these variants is caused by higher D-glucose isomerase activity due to strongly
296 increased XylA protein levels.
297 In the case of strain Fru^{neg} carrying pPREx2-$xylA_{XC}$, three independent ALE experiments all
298 led to the amino acid exchange W147S in $XylA_{XC.}$ This mutation had no obvious effect on the
299 protein level compared to the native enzyme when analyzed by Western blotting (Figure S13B in
300 the supplemental information online). Since the presence of $XylA_{XC}$-W147S in addition to
301 $IolT1^{G87S}$ or $IolT1^{T351P}$ in strain Fru^{neg} led to accelerated growth in D-fructose minimal medium
302 (Figure 2D-G, Figure 2 in the supplemental information online), the W147S mutation should have
303 a positive effect on the D-glucose isomerase activity of XylA. To test this assumption, His-tagged

304 variants of $XylA_{XC}$ and $XylA_{XC}$-W147S were overproduced in *C. glutamicum* MB001(DE3) using
305 plasmids pPREx5-*xylA*$_{XC}$ and pPREx5-*xylA*$_{XC}$-W147S and purified by Ni-NTA and size exclusion
306 chromatography. Both proteins were purified as homodimers (Figure S14 in the supplemental
307 information online). Enzymatic activity was determined by a discontinuous colorimetric assay for
308 D-glucose and D-xylose as substrates [51]. Native $XylA_{XC}$ revealed a 65-fold higher activity for
309 D-xylose compared to D-glucose with catalytic efficiencies (k_{cat}/K_M) of 45.2 ± 6.7 $s^{-1}M^{-1}$ and 0.7
310 ± 0.1 $s^{-1}M^{-1}$, respectively (Table 3). For the $XylA_{XC}$-W147S enzyme, the k_{cat}/K_M for D-glucose
311 increased by 8.4-fold while the k_{cat}/K_M for D-xylose decreased by 2.6-fold, resulting in a
312 diminished activity for D-xylose, only about three times as high as the activity for D-glucose (Table
313 3). The results confirmed the strongly positive effect of the W147S mutation on the D-glucose
314 isomerase activity of $XylA_{XC}$.

315 To assess whether the catalytic performance of $XylA_{XC}$-W147S could be further improved, we
316 established a modified selection system (Figure S15 in the supplemental information online). It
317 employed the Fru^{neg} strain with the *iolT1*-G87S mutation, thereby alleviating the bottleneck in D-
318 fructose uptake. To enable further optimization of $XylA_{XC}$-W147S activity, expression of the
319 corresponding gene was intentionally limited. For this, we examined the growth of Fru^{neg}-IolT1^{G87S}
320 harboring pPREx2-*xylA*$_{XC}$-W147S in D-fructose minimal medium across a range of IPTG
321 concentrations. Plotting the growth rate as a function of the IPTG concentration revealed a
322 Michaelis-Menten-like relationship, with a K_s value of 19.7 ± 2.4 μM IPTG enabling a half-
323 maximal growth rate (Figure S16 in the supplemental information online). Subsequently, *xylA*$_{XC}$-
324 W147S was subjected to random mutagenesis by error-prone PCR and the resulting mutant library
325 was introduced into the Fru^{neg}-IolT1^{G87S} strain (for details see Supplemental Note 1). In consecutive
326 screenings (Figure S17 and Table S3 in the supplemental information online), a $XylA_{XC}$-W147S
327 variant with an additional G15A mutation was found to further increase the growth rate of Fru^{neg}-

328 IolT1^{G87S} in D-fructose minimal medium. Western blot analysis suggested somewhat higher
329 protein levels of the XylA$_{XC}$-G15A-W147S variant compared to the XylA$_{XC}$-W147S variant
330 (Figure S18 in the supplemental information online). Kinetic analysis of purified XylA$_{XC}$-G15A-
331 W147S revealed a slight improvement (10.2%) of catalytic efficiency for D-glucose compared to
332 XylA$_{XC}$-W147S (Table 3).

333 To explore the structural effects of the W147S and G15A-W147S mutations in XylA$_{XC}$ on the
334 binding of D-glucose, we performed all-atom unbiased MD simulations (for further details see
335 Supplemental Note 2). Computations of effective binding energy revealed improved D-glucose
336 binding caused by the W147S mutation in XylA$_{XC}$ (Figure 5A-B), but did not show considerable
337 changes with the additional G15A mutation (Figure 5C).

338

339 **Production of D-allulose from D-glucose with *C. glutamicum***

340 An efficient microbial conversion of D-glucose to D-allulose can only be realized if D-glucose
341 utilization is abolished. For this purpose, the *C. glutamicum* Fru^{neg} strain was further engineered
342 into a D-glucose-negative strain, which cannot utilize D-glucose as sole carbon source. This was
343 achieved by preventing the phosphorylation of D-glucose *via* deletion of the glucokinase genes *glk*,
344 *ppgK*, and *nanK* and by preventing the oxidation of D-glucose to D-gluconate by a side reaction of
345 inositol dehydrogenases via deletion of the inositol-related gene clusters *iol1* and *iol2* and of *idhA3*
346 (for further details see Supplemental Note 3). The resulting Glu^{neg} strain showed no growth in D-
347 glucose minimal medium (Figure S19 in the supplemental information online).

348 To convert D-glucose to D-allulose based on the Glu^{neg} strain, a suitable D-allulose 3-
349 epimerase was required for the epimerization of D-fructose to D-allulose. The D-allulose 3-
350 epimerases of *Agrobacterium tumefaciens* (Dae$_{AT}$) and *Arthrobacter globiformis* (Dae$_{AG}$) [52,53]
351 and a D-tagatose 3-epimerase of *Pseudomonas cichorii* (Dte$_{PC}$) [54] were selected, since they

352 showed a high residual activity for D-fructose at 30°C. The corresponding genes were cloned into
353 the expression plasmid pPREx2. The enzymes were initially tested in the Fru^{neg} strain to check for
354 D-allulose formation from D-fructose in a medium containing 20 g/L of D-fructose and 20 g/L of
355 D-glucose, the latter as growth substrate. Dae_{AT} was the most efficient in producing D-allulose
356 from D-fructose, giving a titer of 4.18 ± 0.14 g/L D-allulose corresponding to a yield of 22.3 ±
357 1.1 % (Figure S20 in the supplemental information online) and therefore was choosen for the
358 subsequent studies.

359 For D-allulose synthesis from D-glucose, the plasmids pPREx2-$xylA_{XC}$-dae_{AT}, pPREx2-
360 $xylA_{XC}$-W147S-dae_{AT}, and pPREx2-$xylA_{XC}$-G15A-W147S-dae_{AT} were constructed, which enable
361 simultaneous synthesis of D-glucose isomerase and D-allulose 3-epimerase. After transfer into the
362 Glu^{neg} strain, the recombinants were cultivated in minimal medium with 10 g/L of D-gluconate for
363 biomass formation and 30 g/L of D-glucose for D-allulose formation. With native $XylA_{XC}$ and
364 Dae_{AT} an D-allulose titer of 1.32 ± 0.07 g/L was obtained after 72 h, corresponding to a yield of
365 4.1 ± 0.3 % from D-glucose (Figure 6). With the improved variants $XylA_{XC}$-W147S and $XylA_{XC}$-
366 G15A-W147S, the yield increased to 9.6 ± 0.4 % and 10.2 ± 0.2 %, respectively (Figure 6). In the
367 next step, D-glucose uptake was improved by introducing the G87S mutation into the genomic
368 *iolT1* gene of strain Glu^{neg} resulting in strain Glu^{neg}-$IolT1^{G87S}$. When transformed with pPREx2-
369 $xylA_{XC}$-G15A-W147S-dae_{AT}, this strain produced 3.45 ± 0.14 g/L D-allulose, corresponding to a
370 yield of 10.9 ± 0.4 % (Figure 6).

371 Unexpectedly, during the D-allulose production experiment an increase of the OD_{600}
372 concomitant with accelerated consumption of D-glucose was observed for the producer strains in
373 comparison to the empty vector control (Figure 6), which required further attention. The presence
374 of D-glucose isomerase in strain Glu^{neg} or Glu^{neg}-$IolT1^{G87S}$ was shown to be necessary for this
375 behavior (Figure S21-22 in the supplemental information online), suggesting that the simultaneous

376 presence of D-glucose and D-fructose could enable partial utilization for growth, despite the Glu^{neg}
377 strain background. To elucidate the reason for this behavior, strain Glu^{neg}-IolT1^{G87S} with pPREx2-
378 *xylA*$_{XC}$-W147S was subjected to ALE to obtain clones showing faster growth on D-glucose. In the
379 ALE experiments, the cultures were initially grown with 10 g/L D-gluconate as second carbon
380 source besides 30 g/L D-glucose. Later the D-gluconate content was reduced to 2 g/L and
381 eventually completely omitted (Figure S23A in the supplemental information online). Fast growing
382 clones were obtained in each of two biological replicates (Figure S23B-C in the supplemental
383 information online). Genome sequencing of one clone from each experiment revealed that both
384 carried an identical mutation in the *ptsS* gene, causing the amino acid exchange A129G in the EII
385 transporter PtsS for D-sucrose (Table S4 in the supplemental information online). As *C.*
386 *glutamicum* lacks a gene for D-sucrose synthase that might have formed D-sucrose from NDP-
387 glucose and D-fructose, we speculated that the A129G mutation might reinforce the ability of PtsS
388 to co-transport D-glucose and D-fructose with concomitant formation of D-glucose 6-phosphate
389 which could be used as a growth substrate. Further studies on PtsS-A129G are reported in
390 Supplemental Note 4.

391 To prevent D-glucose utilization by PtsS in D-allulose production, we deleted the *ptsS* gene in
392 Glu^{neg}-IolT1^{G87S}, resulting in the strain Suc^{neg}-IolT1^{G87S}. When transformed with pPREx2-*xylA*$_{XC}$-
393 G15A-W147S-dae$_{AT}$, the absence of PtsS increased the D-allulose titer by 33% compared to the
394 PtsS-positive strain to 4.6 ± 0.25 g/L and the yield by 39% to 15.1 ± 0.5 % (Figure 6). In high-cell-
395 density biotransformations of the Suc^{neg}-IolT1^{G87S} strain with pPREx2-*xylA*$_{XC}$-G15A-W147S-
396 dae$_{AT}$ (for details see Supplemental Methods), where 58 g/L of D-glucose was added to the culture
397 after biomass formation from 60 g/L of D-gluconate, a D-allulose yield of 11.4 ± 0.2 % was
398 obtained (Figure S24 in the supplemental information online).

399

400 **Discussion**

401 The microbial conversion of D-glucose to D-allulose in foods and beverages provides opportunities
402 to significantly reduce their caloric content and thus the health problems associated with
403 consumption of high-caloric sugars. In our study we created strains of *C. glutamicum* that catalyze
404 the conversion of D-glucose to D-allulose in a two-step reaction involving D-glucose isomerase
405 and D-allulose 3-epimerase. The major hurdle was an efficient conversion of D-glucose to D-
406 fructose within the cytoplasm. D-Glucose isomerases usually have K_m values above 100 mM for
407 D-glucose and D-fructose, but the cytoplasmic concentrations in bacteria are much lower since as
408 these sugars are immediately metabolized after uptake. Furthermore, *C. glutamicum* as many other
409 bacteria take up D-glucose and D-fructose via the PTS, which generates the phosphorylated forms
410 of these sugars that do no serve as substrates for D-glucose isomerase. We prevented uptake via
411 the PTS by deleting the EII enzymes for D-glucose, D-fructose, and D-sucrose, and at the same
412 time enabled uptake of D-glucose and D-fructose via the promiscuous transporter IolT1. When
413 expressing D-glucose isomerase genes in this selection strain, a small but distinct growth on D-
414 fructose was observed due to its conversion to D-glucose followed by phosphorylation and
415 degradation. Subjecting these strains to ALE allowed the selection of clones with a strongly
416 enhanced growth rate on D-fructose.

417 Genomic analysis of six independent ALE clones revealed two features that were responsible
418 for the improved growth rate. Two different single amino acid exchanges in IolT1, G87S and
419 T351P, both strongly improved the uptake of D-glucose and D-fructose. This presumably leads to
420 highly elevated cytoplasmic concentrations of these sugars, which in turn strongly increase D-
421 glucose isomerase activity. Molecular dynamics simulations suggest that both amino acid
422 exchanges allosterically affect two helices known to be functionally involved in transport, thereby
423 enhancing D-glucose and D-fructose transport. The second feature was an increase in the D-glucose

424 isomerase activity. In the case of the enzyme from *Arthrobacter* the elevated activity was due to a
425 strongly increased protein level caused by a mutation in the non-coding mRNA region or by an
426 S2F exchange in the XylA protein. In the case of D-glucose isomerase from *X. campestris*, the
427 increased activity was caused by an W147S exchange, which raised the catalytic efficiency for D-
428 glucose almost 9-fold while reducing it at the same time for D-xylose. Molecular dynamics
429 simulations suggest that binding of D-glucose to $XylA_{XC}$ is stabilized by the W147S substitution.
430 The contribution of the IolT1 mutations to faster growth on D-fructose was higher than the
431 contribution the XylA mutations, but the combination of both mutations was necessary to rebuild
432 strains with the same growth rates as the ALE-derived strains.

433 Native IolT1 has been used in numerous studies for the development of strains producing
434 lysine [26], serine [55], shikimate [56], 3-hydroxypropionate [57], noreugenin [58], or hyaluronic
435 acid [59]. The identification of the variants $IolT1^{G87S}$ and $IolT1^{T351P}$ enabling about 10-fold
436 increased uptake rates for D-glucose and D-fructose should be of high interest for future metabolic
437 engineering studies using IolT1 as a tool to enhance the overall sugar uptake rate or to avoid using
438 the PTS, which is disadvantageous for the production of aromatic compounds requiring PEP as
439 precursor for the shikimate pathway. D-Xylose isomerase is used in yeast for bioethanol production
440 from D-xylose [60], a major constituent of hemicellulose. To our knowledge, this enzyme has never
441 been used before in microbial production strains for the conversion of D-glucose to D-fructose.
442 The $XylA_{XC}$-W147S variant identified in our work offers new options to microbially synthesize D-
443 fructose-derived products from D-glucose, which include disacharide sweeteners (e.g. kojibiose,
444 cellobiose) [61,62], dietary supplements (e.g. mannose) [63], or even furan-based chemicals (e.g.
445 5-hydroxymethylfurfural) [64].

446 Our approaches to engineer a D-glucose-negative strain of *C. glutamicum* turned out to be
447 quite challenging, as suppressor mutants rapidly evolved from strains lacking PtsG and the

448 glucokinases Glk and PpgK. We revealed that inactivating mutations in the genes for the
449 transcriptional repressors IolR and IhtR led to the derepression of their target genes, which include
450 several genes for inositol dehydrogenases[23] that can catalyze the oxidation of D-glucose to D-
451 gluconate as a side-reaction and thereby enable growth. Only after deletion of the inositol
452 dehydrogenase genes a D-glucose-negative strain for D-allulose production was obtained. Many
453 bacteria use D-glucose dehydrogenases for D-glucose metabolization via D-gluconate, such as
454 *Pseudomonas putida* [65] or *Gluconobacter oxydans* [66]. *C. glutamicum* does not possess such
455 dedicated enzymes, but can easily obtain the corresponding activity by inducing inositol
456 dehydrogenases, as shown in our work.

457 Another surprising observation during our study was that the D-glucose-negative strain
458 regained the ability to grow with D-glucose when it expressed D-glucose isomerase. The molecular
459 basis of this phenotype was disclosed by ALE experiments selecting for faster growth of the strain,
460 which revealed the amino acid exchange A129G in PtsS, the EII transporter for D-sucrose. We
461 therefore speculate that PtsS might also have a weak ability to co-transport of D-glucose and D-
462 fructose instead of D-sucrose, forming D-glucose 6-phosphate which can be used for growth. This
463 ability could be enhanced by the A129G mutation, as supported by molecular dynamics
464 simulations. Further studies are needed to follow this feature of PtsS.

465 By deleting *ptsS* in the D-glucose-negative strain the utilization of D-glucose for growth in the
466 presence of D-glucose isomerase could be largely avoided, which increased the D-allulose yield to
467 15%. This value, limited by the reversibility of the D-glucose isomerase and D-allulose 3-
468 epimerase reactions, corresponds to the one obtained with immobilized enzymes at high
469 temperatures of about 60°C, but avoids enzyme purification and immobilization. Furthermore, in
470 high-cell-density biotransformations a comparable D-allulose yield of ~12% was obtained.

471 In conclusion, we provide novel microbial catalysts for the efficient one-pot conversion of D-
472 glucose to D-allulose at 30°C, offering new opportunities for reducing the caloric content of foods
473 and beverages containing D-sucrose or HFCS. Future studies will focus on further engineering of
474 our production strain to enable also the conversion of D-sucrose to D-allulose.
475

476 **Methods**

477 **Bacterial strains, plasmids and growth conditions**

478 All bacterial strains and plasmids used in this work are listed in Table 4. Cloning was performed
479 with *Escherichia coli* DH5α as host. Cultivation of *E. coli* was performed in lysogeny broth (LB)
480 medium or on LB agar plates at 37°C with 50 µg/mL kanamycin, if cells were transformed with a
481 plasmid. *C. glutamicum* was cultivated in brain heart infusion (BHI) medium or on BHI agar plates
482 at 30°C, supplemented with 25 µg/mL and 15 µg/mL kanamycin if carrying a pPREx2 and
483 pK19*mobsacB* plasmid, respectively.
484

485 **Recombinant DNA work and construction of deletion mutants**

486 All plasmids and oligonucleotides used in this study are listed in Table 4 and Table S5 in the
487 supplemental information online, respectively. All D-glucose isomerase (*xylA*), D-allulose 3-
488 epimerase (*dae*), and D-tagatose 3-epimerase (*dte*) genes were ordered in a codon-optimized form
489 for *C. glutamicum* from Life Technologies (Carlsbad, USA). Standard cloning procedures such as
490 PCR, DNA restriction and Gibson assembly were performed according to established protocols
491 [67,68]. Transformation of *E. coli* was performed according to a standard heat-shock protocol [69],
492 while transformation of *C. glutamicum* was conducted via electroporation [70]. Deletion of genes
493 or integration of mutations into the genome of *C. glutamicum* were performed via double
494 homologous recombination using pK19*mobsacB*-based plasmids [71]. Confirmation of deletions

495 or mutations was obtained via colony PCR, using oligonucleotides annealing up- and downstream
496 of the targeted genomic area. To verify the successful integration of mutations, the amplified
497 colony PCR product was additionally sequenced. Expression of selected genes in *C. glutamicum*
498 was performed with the vectors pPREx2 or pPREx5 using a *tac* promoter. The gene of interest was
499 cloned downstream of the consensus ribosome binding site (RBS) of *C. glutamicum* of the
500 respective plasmid. Gene expression was induced by addition of 1 mM or 25 µM isopropyl-β-D-
501 thiogalactoside (IPTG).
502

503 **Growth experiments in BioLector microcultivation systems**

504 For micro-scale cultivations of *C. glutamicum*, the BioLector I, II or XT instruments (Beckman
505 Coulter, Brea, USA) were used. Growth in this system was measured online as scattered light at
506 620 nm with a signal gain factor of 2, 4 or 10 with the BioLector I, II or XT, respectively [31].
507 Cultivations were performed in a 48-well FlowerPlate (Beckman Coulter, Brea, USA) by using
508 defined CGXII medium [72] with 0.03 g/L protocatechuic acid and usually 40 g/L D-glucose, D-
509 fructose or D-sucrose. If the strains carried expression plasmids, 1 mM IPTG and 25 µg/mL
510 kanamycin were added to the medium. Inoculations were individually prepared to reach an initial
511 OD_{600} of 0.5 or 5. BioLector cultivations were performed at 30°C, 1200 rpm and 85% humidity.
512

513 **Adaptive laboratory evolution (ALE)**

514 ALE experiments for the evolution of D-glucose isomerases were prepared in 24-well plates
515 (Porvair Sciences, King's Lynn, UK) containing 5 ml CGXII medium with 40 g/L of D-fructose,
516 25 µg/mL kanamycin and 1 mM IPTG. The plates were shaken at 30°C and 900 rpm in a Multitron
517 shaker (Infors HT, Einsbach, Germany). For evolution of the D-glucose isomerase of *Xanthomonas*
518 *campestris* the first two transfers into fresh medium were performed after 5 days of cultivation with

519 an initial OD_{600} of 7.5. Afterwards, the initial OD_{600} was lowered to 5 and the cultivation time was
520 increased to 15 days. After three more consecutive cultivations, the experiment was stopped. For
521 evolution of the D-glucose isomerase of *Arthrobacter* strain N.R.R.L B3728, the ALE was started
522 at an OD_{600} of 5 with a cultivation time of 15 days. After three rounds of cultivation, the experiment
523 was terminated. ALE experiments for the evolution of the Glu^{neg}-IolT1-G87S strain were
524 performed in 100 mL baffled shake flasks. Initially, CGXII medium containing 10 g/L D-gluconate
525 and 30 g/L D-glucose was used. The initial OD_{600} was set to 0.5 and the cultivation time to 3 days.
526 After three rounds of cultivation, the medium composition was changed to 2 g/L D-gluconate and
527 30 g/L D-glucose for one cultivation of 3 days, whereupon the CGXII composition was again
528 changed to solely 30 g/L of D-glucose for the last 3 days of cultivation.
529
530 **Analysis of D-glucose isomerase protein levels**
531 Investigation of intracellular protein levels was performed via semi-dry Western blot analysis. For
532 this, C-terminally Strep-tagged protein variants of selected candidates were produced in the Fru^{neg}
533 strain by using pPREx2 plasmid constructs (Table 4). Cultivation of strains was conducted in
534 100 mL baffled shake flasks containing 10 mL CGXII medium with 10 g/L of D-glucose, 25 µg/mL
535 kanamycin and 1 mM IPTG for 24 h at 30°C and 130 rpm in a Minitron shaker (Infors HT,
536 Einsbach, Germany). Cells were harvested at 4000 *g* for 30 min, resuspended in PBS and lysed via
537 ceramic beads homogenization in the Precellys® 24 (Avantor, Radnor, USA). Cell debris of whole
538 cell lysates was removed via centrifugation at 20.000 *g* for 10 min to obtain soluble protein
539 fractions. 50 µg of each protein fraction was separated via SDS-PAGE and blotted on a
540 nitrocellulose membrane according to standard procedures [67]. After blocking unspecific and
541 biotinylated protein binding to the membrane via a skim milk and avidin solution, respectively,

542 Strep-tagged proteins were then visualized by a Strep-Tactin-HRP conjugate-based assay (IBA
543 Lifesciences, Göttingen, Germany).
544
545 **Production and purification of D-glucose isomerase variants**
546 Production of $XylA_{XC}$ variants was achieved by using *C. glutamicum* MB001(DE3) strains
547 carrying pPREx5 derivatives with the desired $xylA_{XC}$ variant. BHI medium was used for cultivation,
548 which was inoculated to an OD_{600} of 0.5. Target gene expression was induced with 1 mM IPTG
549 after 4 h of cultivation at 30°C and 130 rpm. After 24 h of cultivation, cells were harvested by
550 centrifugation (4000*g*, 15 min, 4°C) and stored at -80°C for further use.
551 For cell lysis, cells were resuspended in 4 mL lysis buffer (20 mM Tris-HCl pH 7.9, 500 mM NaCl,
552 5% (v/v) glycerol) per g cell wet weight containing cOmplete EDTA-free protease inhibitor
553 (Roche, Basel, Switzerland) and lysed via the Multi Cycle Cell Disruptor (Constant Systems,
554 Daventry, UK). Cell debris was removed via centrifugation (5000*g*, 30 min, 4°C) and filtration of
555 the supernatant via Filtropur 0.2 µm filters (Sartorius, Göttingen, Germany). The soluble protein
556 fraction was then loaded on a HisTrap HP column (GE Healthcare, Chicago, USA) and His-tagged
557 proteins were eluted with 500 mM imidazole in elution buffer (20 mM Tris-HCl pH 7.9, 500 mM
558 NaCl, 5% (v/v) glycerol, 500 mM imidazole). The resulting His-tagged $XylA_{XC}$ proteins were
559 further purified by size exclusion chromatography using a Superdex 200 10/300 GL column (GE
560 Healthcare, Chicago, USA) via isocratic elution with enzyme assay buffer (200 mM $NaPO_4$ pH
561 7.5, 10 mM $MgCl_2$). Protein concentrations were determined with the Bradford assay [73].
562
563 **D-Glucose isomerase activity assay**
564 D-Glucose isomerase activity was detected by measuring D-fructose or D-xylulose formed by
565 isomerization of D-glucose or D-xylose, respectively. For this, a molybdosilicate-dependent

566 colorimetric assay was used [51], where the reduction of D-fructose or D-xylulose by Mo(VI)
567 species resulted in a color change from yellow to blue, which was quantified at 750 nm with a
568 Tecan Infinite M200 Pro microplate reader (Männedorf, Switzerland). The staining reaction was
569 initiated by mixing samples obtained from the isomerization reaction with the 20-fold volume of
570 reaction solution (50 mM Na_2SiO_3, 600 mM Na_2MoO_4, 0.95 M HCl pH 4.5) followed by incubation
571 for 30 min at 70°C. For the isomerization reaction, samples with varying D-glucose (25-1000 mM)
572 and D-xylose (5-750 mM) concentrations were prepared in enzyme assay buffer (200 mM $NaPO_4$
573 pH 7.5, 10 mM $MgCl_2$). The reaction was started by adding 12.5-50 µg of purified D-glucose
574 isomerase for D-glucose isomerization and 0.25-10 µg for D-xylose isomerization. Each reaction
575 was conducted in a final volume of 500 µL at 30°C for 24-48 h. Samples were taken after various
576 time points over this period and mixed with 1/5 volume of 1 M HCl to quench the reaction. After
577 the complete reaction was terminated, quenched samples were used for the colorimetric assay.
578

579 **D-Allulose production experiments**

580 Production experiments for the conversion of either D-fructose or D-glucose to D-allulose were
581 performed with 25 mL CGXII medium in 500 mL baffled shake flasks, which were incubated at
582 30°C and 130 rpm over 72 h. For cultivation of Fru^{neg} strains, overnight precultures were prepared
583 in test tubes in BHI and CGXII medium with 20 g/L D-glucose and 25 µg/mL kanamycin. The
584 main culture was prepared in CGXII medium with 20 g/L of D-glucose and 20 g/L of D-fructose,
585 1 mM IPTG and 25 µg/mL kanamycin. For Glu^{neg} strains, preparation of precultures was similar
586 to Fru^{neg} strains, except that 20 g/L D-glucose was exchanged by 20 g/L D-gluconate in BHI and
587 CGXII medium. Main cultures were prepared in CGXII medium with 10 or 15 g/L of D-gluconate
588 and 30 g/L of D-glucose, 1 mM IPTG and 25 µg/mL kanamycin. In each case, cultivations were
589 started by inoculating the medium to an initial OD_{600} of 0.5. Samples of the supernatant were taken

590 after 12-24 h, used for OD_{600} measurement, filtered with 0.2 µm Whatman Puradisc 13 (Cytiva,
591 Marlborough, USA) and stored at -20 °C for further usage.
592
593 **Metabolite quantification via HPLC**
594 Filtered samples taken from the production experiments were diluted 1:4 or 1:8 with deionized
595 water and used for HPLC analysis. Sugars such as D-fructose, D-glucose, and D-allulose were
596 separated and quantified using a Carbo-Pb Guard Cartridge (Phenomenex, Aschaffenburg,
597 Germany) and a Metab-Pb 250 × 7.8 mm column (ISERA, Düren, Germany) in an Agilent LC-
598 1100 system (Agilent Technologies, Santa Clara, USA). For each analysis, 5 µL of sample was
599 injected into the system and separated at 80°C for 45 min with a flow rate of 0.6 mL/min with
600 double-distilled water filtered through a 0.2 µm filter. A refraction index detector operating at 35°C
601 was used for the detection of sugars. Sugar concentrations of samples were measured via a
602 calibration curve, obtained from sugar standards with concentrations of 1 g/L, 2.5 g/L, 5 g/L, and
603 10 g/L of D-glucose, D-fructose and D-allulose. Organic acids such as D-gluconate, acetate or L-
604 lactate were separated and quantified using a Carbo-H Guard Cartridge and a Rezex ROA –
605 Organic acid H^+ 300 × 7.8 mm column (Phenomenex, Aschaffenburg, Germany) in an Agilent LC-
606 1260 system. 10 µL of sample were injected into the system for each analysis and separated at
607 70°C for 40 min with a flow rate of 0.5 mL/min with 5 mM of sulfuric acid. Organic acids were
608 detected via an Agilent Diode Array Detector at 215 nm. Concentration of organic acids were
609 quantified via a calibration curve, obtained from standards with concentrations of 1 g/L, 2.5 g/L,
610 5 g/L and 10 g/L of D-gluconate, acetate and L-lactate.
611
612 **Preparation of IolT1 starting structures**

613 To our knowledge, there is no experimentally resolved 3D structure of IolT1 from *C. glutamicum*
614 available. The starting structures for MD simulations of the different IolT1 states were thus
615 modeled using TopModel [74] and the structures available in the Protein Data Bank [75] with PDB
616 IDs 4ZWC, 4ZW9, 4JA3, and 4YB9 of the GLUT3 transporters in *H. sapiens*, the XylE transporter
617 in *E. coli*, and the bovine GLUT5 transporter [42] as single templates for the outward-open,
618 outward-occluded, inward-occluded, and inward-open conformations, respectively. The target
619 sequence for IolT1 has Uniprot ID Q8NTX0 [76]. The quality of the models was assessed with
620 TopScoreSingle (Table S2 in the supplemental information online) [77].

621 The substitutions G87S, T351P, and G87S-T351P were introduced into IolT1 using FoldX
622 [35], and the stability of the variants was evaluated in terms of the change in the folding free energy
623 ($\Delta\Delta G$) with respect to the wildtype [78], as done for other bacterial membrane proteins [36]. Single
624 amino acid substitutions were performed 10 times for the respective residue and the results were
625 averaged. If the average $\Delta\Delta G > 3$ kcal/mol, the substitution is considered destabilizing [79] and is
626 not further pursued (Table S2 in the supplemental information online).

627 In an aqueous solution of 20°C, D-fructose exists as an equilibrium of ~70% β-D-
628 fructopyranose (BFP), ~23% of β-D-fructofuranose (BFF), and smaller percentages of the open
629 chain and cyclic α-anomers [80]. Considering the low growth rate of cells containing IolT1 for D-
630 fructose (Figure 3), we hypothesized that this originates from the transport of BFF, which is less
631 prevalent in solution. Accordingly, we prepared the BFF structure starting from its canonical
632 SMILES using the fixpka option in OpenEye [81]. The most favorable conformer was generated
633 using Omega 4.1.1.1 [82] and the flag -maxconfs = 1. BFF docking to IolT1 was performed using
634 Autodock-3.0.5 [83] with the objective function DrugScore [84]. The selected pose represents the
635 most populated cluster.

636 In an aqueous solution of 20°C, D-glucose exists as an equilibrium of ~36% α-D-
637 glucopyranose (AGP) and ~64% β-D-glucopyranose (BGP) [85]. The more prevalent BGP
638 structure is available in the Protein Data Bank (PDB ID 4ZW9) bound to human GLUT3 in the
639 outward-occluded configuration [86]. After the superposition of the available protein structure with
640 our generated model (RMSD = 0.3 Å), the bound pose of BGP was extracted and merged with the
641 obtained model. Parallely, BGP was docked into the model, using the same protocol employed for
642 BFF. The two BGP structures have a ligand dRMSD < 1.0 Å. We decided to use the BGP pose
643 from the superpositioning and merging as the starting configuration.

644 The partial atomic charges of the two carbohydrate configurations were determined by first
645 computing electrostatic potentials with Gaussian 16 [87] at the HF/6-31G level of theory and then
646 performing a restrained fitting according to the RESP procedure [88,89]. The protonation states of
647 protein residues were adjusted according to pH 7.4 using the Epik routine [90-92] in Maestro [93].
648 The two unbound (outward-open, inward-open) and four bound (outward-occluded and inward-
649 occluded, both with BGP and BFF) IolT1 conformations were embedded into a membrane
650 composed of phosphatidylglycerol 16:0-18:1, cardiolipin 16:0-18.1, and phosphatidylinositol 16:0-
651 18:1 in a ratio of 6:2:1 using the PPM server [34] and solvated using PACKMOL-Memgen [94,95].
652 The membrane composition resembles that of the native inner membrane of *C. glutamicum* [37,96].
653 A distance of at least 15 Å between the protein or membrane in the z-direction and the solvent box
654 boundaries was kept. To obtain a neutral system, counter ions were added that replaced solvent
655 molecules (KCl 0.15 M). A total of 16 independent starting configurations were generated and are
656 listed in Table S2 in the supplemental information online.

657

658 **Unbiased molecular dynamics (MD) simulations of IolT1 configurations, XylA$_{XC}$ and PtsS**

659 The GPU particle mesh Ewald implementation from the AMBER23 suite of molecular simulations
660 programs [97] with the ff19SB [98], Lipid21 [99], and the GLYCAM-06j [100] forcefields for the
661 protein, membrane lipids, and carbohydrate ligands, respectively, were used; water molecules and
662 ions were parametrized using the OPC3POL model [101,102] and the Li and Merz 12-6 ions
663 parameters [103-105]. For each configuration in Table S2 and Table S6 in the supplemental
664 information online, five independent MD simulations of 2 μs length were performed. Covalent
665 bonds to hydrogens were constrained with the SHAKE algorithm [106], and the hydrogen masses
666 were repartitioned [107], allowing the use of a time step of 4 fs. Details of the thermalization of
667 the simulation systems are given below. All unbiased MD simulations of IolT1 showed structurally
668 rather invariant protein structures and membrane phases as evidenced by electron density
669 calculations (Figure S4-9 in the supplemental information online). The overall nofit-RMSD of β-
670 D-glucopyranose (BGP) and β-D-fructofuranose (BFF) revealed structurally stable binding poses
671 across different replicas for the outward-occluded and inward-occluded configurations (Figure S10
672 in the supplemental information online). The unbiased MD simulations of $XylA_{XC}$ yielded
673 structurally rather invariant protein structures and stable binding poses of the ligands (Figure S25
674 in the supplemental information online). All unbiased MD simulations of PtsS showed structurally
675 rather invariant protein structures and membrane phases as evidenced by electron density
676 calculations (Figure S26-27 in the supplemental information online). The overall nofit-RMSD of
677 BGP, BFF, D-sucrose and BGP/BFF revealed structurally stable binding poses across different
678 replicas for the wild type and A129G mutant configurations (Figure S28 in the supplemental
679 information online).
680
681 **MM-PBSA calculations to assess β-D-glucopyranose (BGP)/β-D-fructofuranose (BFF)**
682 **binding to IolT1, BGP binding to $XylA_{XC}$, and carbohydrate binding to PtsS**

683 MM-PBSA (Molecular Mechanics Poisson-Boltzmann Surface Area) calculations were conducted
684 to determine the effective binding energies (ΔG_{eff}) of BGP/BFF binding to IolT1, BGP binding to
685 $XylA_{XC}$, and the binding of multiple carbohydrates to PtsS. Note that MM-PBSA computations
686 were performed to provide qualitative insight into the relative effects of mutations on ligand
687 binding and protein stability. For further details on the scope of MM-PBSA computations, see
688 Supplemental Note 2. These calculations were performed for IolT1, $XylA_{XC}$, and PtsS in the
689 wildtype state and the proposed mutants, utilizing the last 1.5 µs of the trajectories from unbiased
690 MD simulations. The first 500 ns were considered as part of the thermalization phase. Ligand
691 binding poses were identified as those exhibiting an RMSD < 1.5 Å compared to the first frame of
692 each respective production run. To compute the average effective binding energy of each ligand
693 with the respective system within the ensemble of the unbiased MD frames, we employed
694 MMPBSA.py [108]. This was done using dielectric constants of 1.0 for the protein and 80.0 for
695 the solvent. For IolT1, the cumulative effective binding energy of two specific regions of interest
696 ($\Delta G_{eff,r}$ for residues 290-306 and residues 390-401) was also calculated. For $XylA_{XC}$ and PtsS, the
697 effective binding energy computations were performed for the two monomers, and the results were
698 averaged. The reported error bars represent the SEM and, therefore, the precision of the method
699 across production trajectories and replica systems and not its accuracy. The computations were
700 converged, as evidenced by the comparison between the first and second halves of the trajectories
701 (Figure S29-30 in the supplemental information online).
702

703 **Data and code availability**

704 The data generated in this study are provided in the manuscript, in the supplemental information,
705 and in the repository researchdata.hhu.de at https://researchdata.hhu.de/handle/entry/205

706 (https://doi.org/10.25838/d5p-88). The manuscript does not report original code. Any additional

707 data can be obtained from the corresponding author upon reasonable request.

708

References

1. Rippe, J.M. and Angelopoulos, T.J. (2016) Relationship between Added Sugars Consumption and Chronic Disease Risk Factors: Current Understanding. *Nutrients* 8.
2. Carocho, M. *et al.* (2017) Sweeteners as food additives in the XXI century: A review of what is known, and what is to come. *Food Chem Toxicol* 107, 302-317.
3. DuBois, G.E. and Prakash, I. (2012) Non-caloric sweeteners, sweetness modulators, and sweetener enhancers. *Annu Rev Food Sci Technol* 3, 353-380.
4. Iida, T. *et al.* (2010) Failure of D-psicose absorbed in the small intestine to metabolize into energy and its low large intestinal fermentability in humans. *Metabolism* 59, 206-214.
5. Han, Y. *et al.* (2018) A preliminary study for evaluating the dose-dependent effect of D-allulose for fat mass reduction in adult humans: a randomized, double-blind, placebo-controlled trial. *Nutrients* 10, 160.
6. Franchi, F. *et al.* (2021) Effects of D-allulose on glucose tolerance and insulin response to a standard oral sucrose load: results of a prospective, randomized, crossover study. *BMJ Open Diab Res Care* 9, e001939.
7. Koch, T.J. *et al.* (2019) Synthesis of D-allulose. *Patent US20190315790*.
8. Bhosale, S.H. *et al.* (1996) Molecular and industrial aspects of glucose isomerase. *Microbiol. Rev.* 60, 280-300.
9. Tewari, Y.B. and Goldberg, R.N. (1984) Thermodynamics of the conversion of aqueous glucose to fructose. *J Solution Chem* 13, 523-547.
10. Zhu, G.P. *et al.* (1999) Increasing the thermostability of D-xylose isomerase by introduction of a proline into the turn of a random coil. *Protein Eng* 12, 635-638.
11. Dekker, K. *et al.* (1991) Xylose (glucose) isomerase gene from the thermophile *Thermus thermophilus*: cloning, sequencing, and comparison with other thermostable xylose isomerases. *J Bacteriol* 173, 3078-3083.
12. Vieille, C. *et al.* (1995) xylA cloning and sequencing and biochemical characterization of xylose isomerase from *Thermotoga neapolitana*. *Appl Environ Microbiol* 61, 1867-1875.
13. Zhang, W. *et al.* (2016) Recent advances in D-allulose: physiological functionalities, applications, and biological production. *Trends Food Sci* 54, 127-137.
14. Chen, X. *et al.* (2017) Production of D-psicose from D-glucose by co-expression of D-psicose 3-epimerase and xylose isomerase. *Enzyme Microb Technol* 105, 18-23.
15. Chen, X. *et al.* (2022) One pot cascade biosynthesis of D-allulose from D-glucose and its kinetic modelling. *Chem Eng Sci* 248, 117167.
16. Men, Y. *et al.* (2014) Co-expression of D-glucose isomerase and D-psicose 3-epimerase: development of an efficient one-step production of D-psicose. *Enzyme Microb Technol* 64-65, 1-5.
17. Eggeling, L. and Bott, M. (2005) Handbook of Corynebacterium glutamicum. *CRC Press* Book.
18. Yukawa, H. and Inui, M., eds (2013) *Corynebacterium glutamicum: Biology and Biotechnology* (*Microbiology Monographs*, Springer
19. Blombach, B. and Seibold, G.M. (2010) Carbohydrate metabolism in *Corynebacterium glutamicum* and applications for the metabolic engineering of L-lysine production strains. *Appl Microbiol Biotechnol* 86, 1313-1322.
20. Moon, M.-W. *et al.* (2005) Analyses of enzyme II gene mutations for sugar transport and heterologous expression of fructokinase gene in *Corynebacterium glutamicum* ATCC 13032. *FEMS Microbiol Lett* 244, 259-266.

755 21. Engels, V. *et al.* (2008) ScrB (Cg2927) is a sucrose-6-phosphate hydrolase essential for
756 sucrose utilization by *Corynebacterium glutamicum*. *FEMS Microbiol Lett* 289, 80-89.
757 22. Krings, E. *et al.* (2006) Characterization of myo-inositol utilization by Corynebacterium
758 glutamicum: the stimulon, identification of transporters, and influence on L-lysine
759 formation. *J Bacteriol* 188, 8054-8061.
760 23. Ramp, P. *et al.* (2022) Physiological, biochemical, and structural bioinformatic analysis of
761 the multiple inositol dehydrogenases from *Corynebacterium glutamicum*. *Microbiol Spectr*
762 10, e01950-01922.
763 24. Baumchen, C. *et al.* (2009) Myo-inositol facilitators IolT1 and IolT2 enhance D-mannitol
764 formation from D-fructose in Corynebacterium glutamicum. *FEMS Microbiol Lett* 290,
765 227-235.
766 25. Ikeda, M. *et al.* (2011) Identification and application of a different glucose uptake system
767 that functions as an alternative to the phosphotransferase system in *Corynebacterium*
768 *glutamicum*. *Appl. Microbiol. Biotechnol.* 90, 1443-1451.
769 26. Lindner, S.N. *et al.* (2011) Phosphotransferase system-independent glucose utilization in
770 *Corynebacterium glutamicum* by inositol permeases and glucokinases. *Appl. Environ.*
771 *Microbiol.* 77, 3571-3781.
772 27. Lindner, S.N. *et al.* (2010) Cg2091 encodes a polyphosphate/ATP-dependent glucokinase
773 of *Corynebacterium glutamicum*. *Appl Microbiol Biotechnol* 87, 703-713.
774 28. Park, S.-Y. *et al.* (2000) Characterization of *glk*, a gene coding for glucose kinase of
775 *Corynebacterium glutamicum*. *FEMS Microbiol Lett* 188, 209-215.
776 29. Klaffl, S. *et al.* (2013) Complex regulation of the phosphoenolpyruvate carboxykinase gene
777 *pck* and characterization of its GntR-type regulator IolR as a repressor of *myo*-inositol
778 utilization genes in *Corynebacterium glutamicum*. *J Bacteriol* 195, 4283-4296.
779 30. Brüsseler, C. *et al.* (2018) The myo-inositol/proton symporter IolT1 contributes to D-xylose
780 uptake in *Corynebacterium glutamicum*. *Bioresour Technol* 249, 953-961.
781 31. Kensy, F. *et al.* (2009) Validation of a high-throughput fermentation system based on online
782 monitoring of biomass and fluorescence in continuously shaken microtiter plates. *Microb.*
783 *Cell Fact.* 8, 31.
784 32. Bäumchen, C. *et al.* (2009) *Myo*-Inositol facilitator IolT1 and IolT2 enhance D-mannitol
785 formation from D-fructose in *Corynebacterium glutamicum*. *FEMS Microbiol Lett* 290,
786 227-235.
787 33. Xu, J.-Z. *et al.* (2020) Metabolic engineering of carbohydrate metabolism systems in
788 *Corynebacterium glutamicum* for improving the efficiency of L-lysine production from
789 mixed sugars. *Microb Cell Fact* 19, 39.
790 34. Lomize, M.A. *et al.* (2012) OPM database and PPM web server: resources for positioning
791 of proteins in membranes. *Nucleic Acids Res* 40, D370-376.
792 35. Schymkowitz, J. *et al.* (2005) The FoldX web server: an online force field. *Nucleic Acids*
793 *Res* 33, W382-388.
794 36. Gentile, R. *et al.* (2024) Molecular mechanisms underlying medium-chain free fatty acid-
795 regulated activity of the phospholipase PlaF from *Pseudomonas aeruginosa*. *Jacs Au* 4,
796 958-973.
797 37. Klatt, S. *et al.* (2018) Identification of novel lipid modifications and intermembrane
798 dynamics in *Corynebacterium glutamicum* using high-resolution mass spectrometry. *J*
799 *Lipid Res* 59, 1190-1204.
800 38. Pfleger, C. *et al.* (2017) Ensemble- and rigidity theory-based perturbation approach to
801 analyze dynamic allostery. *J Chem Theory Comput* 13, 6343-6357.

802 39. Pfleger, C. *et al.* (2013) Global and local indices for characterizing biomolecular flexibility
803 and rigidity. *J Comput Chem* 34, 220-233.
804 40. Preising, M.N. *et al.* (2019) Biallelic mutation of human SLC6A6 encoding the taurine
805 transporter TAUT is linked to early retinal degeneration. *FASEB J* 33, 11507-11527.
806 41. Wifling, D. *et al.* (2019) Basal histamine H_4 receptor activation: Agonist mimicry by the
807 diphenylalanine motif. *Chemistry* 25, 14613-14624.
808 42. Drew, D. *et al.* (2021) Structures and general transport mechanisms by the Major Facilitator
809 Superfamily (MFS). *Chem Rev* 121, 5289-5335.
810 43. Pao, S.S. *et al.* (1998) Major facilitator superfamily. *Microbiol Mol Biol Rev* 62, 1-34.
811 44. Acevedo-Rocha, C.G. *et al.* (2021) Pervasive cooperative mutational effects on multiple
812 catalytic enzyme traits emerge via long-range conformational dynamics. *Nat Commun* 12,
813 1621.
814 45. Klingenberg, M. (2005) Ligand-protein interaction in biomembrane carriers. The induced
815 transition fit of transport catalysis. *Biochemistry* 44, 8563-8570.
816 46. Bogdanov, M. and Dowhan, W. (1995) Phosphatidylethanolamine is required for *in-vivo*
817 function of the membrane-associated lactose permease of *Escherichia coli*. *J Biol Chem*
818 270, 732-739.
819 47. Kaback, H.R. and Guan, L. (2019) It takes two to tango: The dance of the permease. *J Gen*
820 *Physiol* 151, 878-886.
821 48. Bivona, L. *et al.* (2010) Influence of the second amino acid on recombinant protein
822 expression. *Protein Expr Purif* 74, 248-256.
823 49. Seo, S.W. *et al.* (2013) Predicitve design of mRNA translation initiation region to control
824 prokaryotic translation efficiency. *Metab Eng* 15, 67-74.
825 50. Chen, Y.-L. and Wen, J.-D. (2022) Translation initiation site of mRNA is selected through
826 dynamic interaction with the ribosome. *Proc Natl Acad Sci USA* 119, e2118099119.
827 51. Katano, H. *et al.* (2015) Colorimetric determination of fructose for the high-throughput
828 microtiter plate assay of glucose isomerase. *Biosci Biotech Biochem* 79, 1057-1060.
829 52. Kim, H.-J. *et al.* (2006) Characterization of an *Agrobacterium tumefaciens* D-psicose 3-
830 epimerase that converts D-fructose to D-psicose. *Appl Environ Microbiol* 72, 981-985.
831 53. Yoshihara, A. *et al.* (2017) Purification and characterization of D-allulose 3-epimerase
832 derived from *Arthrobacter globiformis* M30, a GRAS microorganism. *J Biosci Bioeng* 123,
833 170-176.
834 54. Itoh, H. *et al.* (1994) Purification and characterization of D-tagatose 3-epimerase from
835 *Pseudomonas* sp. ST-24. *Biosci Biotech Biochem* 58, 2168-2171.
836 55. Zhang, X. *et al.* (2019) Rewiring the central metabolic pathway for high-yield L-serine
837 production in *Corynebacterium glutamicum* by using glucose. *Biotechnol J* 14, e1800497.
838 56. Kogure, T. *et al.* (2016) Metabolic engineering of *Corynebacterium glutamicum* for
839 shikimate overproduction by growth-arrested cell reaction. *Metab. Eng.* 38, 204-216.
840 57. Chen, Z. *et al.* (2017) Metabolic engineering of *Corynebacterium glutamicum* for the
841 production of 3-hydroxypropionic acid from glucose and xylose. *Metab. Eng.* 39, 151-158.
842 58. Milke, L. *et al.* (2019) Tailoring *Corynebacterium glutamicum* towards increased malonyl-
843 CoA availability for efficient synthesis of the plant pentaketide noreugenin. *Microb. Cell*
844 *Fact.* 18, 71.
845 59. Du, Y. *et al.* (2021) Indirect pathway metabolic engineering strategies for enhanced
846 biosynthesis of hyaluronic acid in engineered *Corynebacterium glutamicum*. *Front. Bioeng.*
847 *Biotechnol.* 9, 768490.

60. Kuyper, M. *et al.* (2005) Metabolic engineering of a xylose-isomerase-expressing *Saccharomyces cerevisiae* strain for rapid anaerobic xylose fermentation. *FEMS Yeast Res.* 5, 399-409.
61. Beerens, K. *et al.* (2017) Biocatalytic synthesis of the rare sugar kojibiose: process scale-up and application testing. *J Agric Food Chem* 65, 6030-6041.
62. Inokuma, K. *et al.* (2024) One-pot synthesis of cellobiose from sucrose using sucrose phosphorylase and cellobiose phosphorylase co-displaying *Pichia pastoris* as a reusable whole-cell biocatalyst. *Sci Rep* 14, 18540.
63. Huang, J. *et al.* (2018) Production of D-mannose from D-glucose by co-expression of D-glucose isomerase and D-lyxose isomerase in *Escherichia coli*. *J Sci Food Agric* 98, 4895-4902.
64. You, L. *et al.* (2023) Efficient conversion of glucose to 5-hydroxymethylfurfural by synergetic catalysis of enzymes and chemical catalysts towards potential large-scale continous operation. *Chem Eng J* 459, 141552.
65. An, R. and Moe, L.A. (2016) Regulation of pyrroloquinoline quinone-dependent glucose dehydrogenase activity in the model rhizosphere-dwelling bacterium *Pseudomonas putida* KT2440. *Appl Environ Microbiol* 82, 4955-4964.
66. Hölscher, T. *et al.* (2009) Glucose oxidation and PQQ-dependent dehydrogenases in *Gluconobacter oxydans*. *Journal of molecular microbiology and biotechnology* 16, 6-13.
67. Green, M.R. and Sambrook, J. (2012) Molecular cloning: a laboratory manual, 3rd ed. *Cold Spring Harb Lab. Press, Cold Spring Harbor, NY*.
68. Gibson, D.G. *et al.* (2009) Enzymatic assembly of DNA molecules up to several hundred kilobases. *Nat Methods* 6, 343-345.
69. Hanahan, D. (1983) Studies on transformation of *Escherichia coli* with plasmids. *J Mol Biol* 166, 557-580.
70. van der Rest, M.E. *et al.* (1999) A heat shock following electroporation induces highly efficient transformation of *Corynebacterium glutamicum* with xenogeneic plasmid DNA. *Appl Microbiol Biotechnol* 52, 541-545.
71. Schäfer, A. *et al.* (1994) Small mobilizable multi-purpose cloning vectors derived from the *Escherichia coli* plasmids pK18 and pK19: selection of defined deletions in the chromosome of *Corynebacterium glutamicum*. *Gene* 145, 69-73.
72. Keilhauer, C. *et al.* (1993) Isoleucine synthesis in *Corynebacterium glutamicum*: molecular analysis of the ilvB-ilvN-ilvC operon. *J Bacteriol* 175, 5595-5603.
73. Bradford, M.M. (1976) A rapid and sensitive method for the quanitification of microgram quantities of protein utilizing the principle of protein-dye binding. *Anal Biochem* 72, 248-254.
74. Mulnaes, D. *et al.* (2020) TopModel: Template-based protein structure prediction at low sequence identity using top-down consensus and deep neural networks. *J Chem Theory Comput* 16, 1953-1967.
75. Berman, H.M. *et al.* (2000) The Protein Data Bank. *Nucleic Acids Res.* 28, 235-242.
76. UniProt, C. (2023) UniProt: the Universal Protein Knowledgebase in 2023. *Nucleic Acids Res* 51, D523-D531.
77. Mulnaes, D. and Gohlke, H. (2018) TopScore: Using deep neural networks and large diverse data sets for accurate protein model quality assessment. *J Chem Theory Comput* 14, 6117-6126.
78. Guerois, R. *et al.* (2002) Predicting changes in the stability of proteins and protein complexes: a study of more than 1000 mutations. *J Mol Biol* 320, 369-387.

79. Tokuriki, N. *et al.* (2007) The stability effects of protein mutations appear to be universally distributed. *J Mol Biol* 369, 1318-1332.
80. Benardout, M. *et al.* (2022) Fructose malabsorption: causes, diagnosis and treatment. *Brit. J. Nutr.* 127, 481-489.
81. OEDocking, O. OEDocking 4.3.0.3. Cadence Molecular Sciences, Inc.
82. OpenEye (2019). OMEGA OpenEye Scientific Software,
83. Morris, G.M. *et al.* (1999) Automated docking using a Lamarckian genetic algorithm and an empirical binding free energy function. *J Comput Chem* 19, 1639-1662.
84. Dittrich, J. *et al.* (2019) Converging a knowledge-based scoring function: DrugScore^{2018} *J Chem Inf Model* 59, 509-521.
85. Oliva, L. *et al.* (2019) The anomeric nature of glucose and its implications on its analyses and the influence of diet: Are routine glycaemia measurements reliable enough? *J Endocrinol Metab* 9, 63-70.
86. Deng, D. *et al.* (2015) Molecular basis of ligand recognition and transport by glucose transporters. *Nature* 526, 391-396.
87. Frisch, M.J. *et al.* (2016). Gaussian 16 Rev. C.01.
88. Bayly, C.I. *et al.* (1993) A well-behaved eectrostatic potential based method using charge restraints for deriving atomic charges - the RESP model. *J. Phys. Chem.* 97, 10269-10280.
89. Cornell, W.D. *et al.* (1996) A second generation force field for the simulation of proteins, nucleic acids, and organic molecules *J. Am. Chem. Soc.* 118, 2309-2309.
90. Greenwood, J.R. *et al.* (2010) Towards the comprehensive, rapid, and accurate prediction of the favorable tautomeric states of drug-like molecules in aqueous solution. *J Comput Aided Mol Des* 24, 591-604.
91. Johnston, R.C. *et al.* (2023) Epik: pK_a and protonation state prediction through machine learning. *J Chem Theory Comput* 19, 2380-2388.
92. Shelley, J.C. *et al.* (2007) Epik: a software program for pK_a prediction and protonation state generation for drug-like molecules. *J Comput Aided Mol Des* 21, 681-691.
93. Schrödinger (2023). Maestro. Schrödinger LLC
94. Martinez, L. *et al.* (2009) PACKMOL: a package for building initial configurations for molecular dynamics simulations. *J Comput Chem* 30, 2157-2164.
95. Schott-Verdugo, S. and Gohlke, H. (2019) PACKMOL-Memgen: A simple-to-use, generalized workflow for membrane-protein-lipid-bilayer system building. *J Chem Inf Model* 59, 2522-2528.
96. Özcan, N. *et al.* (2007) Osmolality, temperature, and membrane lipid composition modulate the activity of betaine transporter BetP in *Corynebacterium glutamicum*. *J Bacteriol* 189, 7485-7496.
97. Case, D.A. *et al.* (2023) AmberTools. *J Chem Inf Model* 63, 6183-6191.
98. Tian, C. *et al.* (2020) ff19SB: Amino-acid-specific protein backbone parameters trained against quantum mechanics energy surfaces in solution. *J Chem Theory Comput* 16, 528-552.
99. Dickson, C.J. *et al.* (2022) Lipid21: Complex lipid membrane smulations with AMBER. *J. Chem. Theory Comput.* 18, 1726-1736.
100. Kirschner, K.N. *et al.* (2008) GLYCAM06: a generalizable biomolecular force field. Carbohydrates. *J Comput Chem* 29, 622-655.
101. Xiong, Y. *et al.* (2022) Fast polarizable water model for atomistic simulations. *J Chem Theory Comput* 18, 6324-6333.

941 102. Xiong, Y. *et al.* (2023) Correction to "Fast polarizable water model for atomistic
942 simulations". *J Chem Theory Comput* 19, 377.
943 103. Li, P. *et al.* (2015) Systematic parameterization of monovalent ions employing the
944 nonbonded model. *J Chem Theory Comput* 11, 1645-1657.
945 104. Sengupta, A. *et al.* (2021) Correction to "Parameterization of monovalent ions for the
946 OPC3, OPC, TIP3P-FB, and TIP4P-FB water models". *J Chem Inf Model* 61, 3734-3735.
947 105. Sengupta, A. *et al.* (2021) Parameterization of monovalent ions for the OPC3, OPC, TIP3P-
948 FB, and TIP4P-FB water models. *J Chem Inf Model* 61, 869-880.
949 106. Kräutler, V. *et al.* (2001) A fast SHAKE:: Algorithm to solve distance constraint equations
950 for small molecules in molecular dynamics simulations. *J Comput Chem* 22, 501-508.
951 107. Hopkins, C.W. *et al.* (2015) Long-time-step molecular dynamics through hydrogen mass
952 repartitioning. *J Chem Theory Comput* 11, 1864-1874.
953 108. Miller, B.R. *et al.* (2012) MMPBSA.py: An efficient program for end-state free energy
954 calculations. *J. Chem. Theory Comput.* 8, 3314-3321.
955 109. Baumgart, M. *et al.* (2013) Construction of a prophage-free variant of *Corynebacterium*
956 *glutamicum* ATCC 13032 for use as a platform strain for basic research and industrial
957 biotechnology. *Appl Environ Microbiol* 79, 6006-6015.
958 110. Kortmann, M. *et al.* (2015) A chromosomally encoded T7 RNA polymerase-dependent
959 gene expression system for *Corynebacterium glutamicum*: construction and comparative
960 evaluation at the single-cell level. *Microb Biotechnol* 8, 253-265.
961 111. Ramp, P. *et al.* (2021) Metabolic engineering of *Corynebacterium glutamicum* for
962 production of *scyllo*-inositol, a drug candidate against Alzheimer's disease. *Metab Eng* 67,
963 173-185.
964 112. Bakkes, P.J. *et al.* (2020) Improved pEKEx2-derived expression vector for tightly
965 controlled production of recombinant proteins in *Corynebacterium glutamicum*. *Plasmid*
966 112, 102540.
967 113. Abramson, J. *et al.* (2024) Accurate structure prediction of biomolecular interactions with
968 AlphaFold 3. *Nature* 630, 493-500.

969

Acknowledgments

This project was funded by the Bundesministerium für Bildung und Forschung (BMBF) within the project IMPRES-2 (FKZ 031B1054B), grant to M.B., and, in part, by the Deutsche Forschungsgemeinschaft (DFG, German Research Foundation), project 267205415/CRC1208, grant to H.G. (subproject A03), and, in part, by a grant from the Ministry of Innovation, Science, and Research within the framework of the NRW Strategieprojekt BioSC (No. 313/323-400-002 13). We are grateful for computational support from the "Zentrum für Informations und Medientechnologie" at the Heinrich-Heine-Universität Düsseldorf and the computing time provided by the John von Neumann Institute for Computing (NIC) to H.G. on the supercomputer JUWELS at the Jülich Supercomputing Centre (JSC) (user IDs: VSK33, T1SS). We would like to thank Susana Matamouros for critically reading the manuscript.

Author contributions

A.L. and M.B. designed the study. A.L. generated the wet lab experimental data, while R.G. and H.G. performed the molecular dynamics simulations. C. T. supported the strain constructions and A.W. the HPLC measurements. T. P. evaluated the whole genome sequencing data. M. Ba. contributed to supervision. A.L. and R.G. performed the data work including data curation, formal analysis and statistics and prepared figures and tables. A.L., R.G., H.G., and M.B. drafted the manuscript and were responsible for the final review and editing.

Declaration of interests

The authors declare no competing interests.

993 **Table 1. Plasmid and genome mutations of ALE-derived Fru^{neg} pPREx2-*xylA* strains.**
994

Strain	Location of mutation	Mutation
FAB evo 1	*xylA*$_{AB}$ (plasmid)	S2F
	iolT1 (genome)	G87S
FAB evo 2	pPREx2 (plasmid)	c to t mutation 20 bp upstream of *xylA*$_{AB}$ start codon (c_t)
	iolT1 (genome)	T351P
FAB evo 3	pPREx2 (plasmid)	c to t mutation 20 bp upstream of *xylA*$_{AB}$ start codon (c_t)
	iolT1 (genome)	G87S
FXC evo 1	*xylA*$_{XC}$ (plasmid)	W147S
	iolT1 (genome)	G87S
FXC evo 2	*xylA*$_{XC}$ (plasmid)	W147S
	iolT1 (genome)	G87S
FXC evo 3	*xylA*$_{XC}$ (plasmid)	W147S
	iolT1 (genome)	T351P

995

996

997 **Table 2. Influence of the amino acid exchanges G87S and T351P in IolT1 on μ_{max} and K_s.**
998

Substrate	Strain	μ_{max} (h^{-1})[a]	K_S (mM)[a]
D-Fructose	Fru^{neg} pPREx2-*scrK*	0.032 ± 0.002	106.9 ± 7.6
	Fru^{neg}-IolT1^{G87S} pPREx2-*scrK*	0.329 ± 0.017	80.2 ± 1.8
	Fru^{neg}-IolT1^{T351P} pPREx2-*scrK*	0.336 ± 0.013	72.6 ± 4.2
	Fru^{neg}-IolT1$^{G87S-T351P}$ pPREx2-*scrK*	0.380 ± 0.003	93.3 ± 3.3
D-Glucose	Fru^{neg}	0.296 ± 0.010	18.9 ± 2.8
	Fru^{neg}-IolT1^{G87S}	0.548 ± 0.017	1.9 ± 0.8
	Fru^{neg}-IolT1^{T351P}	0.532 ± 0.010	1.4 ± 0.9
	Fru^{neg}-IolT1$^{G87S-T351P}$	0.519 ± 0.039	4.9 ± 1.5

999 [a] Mean ± S.D. of the sigmoidal non-linear regression fits of three independent replicates

1000

1001 **Table 3. Kinetic parameters of $XylA_{XC}$ variants for the conversion of D-glucose and D-xylose.**

1002

Enzyme variant	D-Glucose[a]			D-Xylose[a]		
	k_{cat} (s^{-1})	K_M (mM)	k_{cat}/K_M (s^{-1} M^{-1})	k_{cat} (s^{-1})	K_M (mM)	k_{cat}/K_M (s^{-1} M^{-1})
$XylA_{XC}$	0.081 ± 0.003	116 ± 8	0.7 ± 0.1	1.48 ± 0.06	33 ± 4	45.2 ± 6.7
$XylA_{XC}$-W147S	0.43 ± 0.03	73 ± 10	5.9 ± 0.4	1.26 ± 0.05	73 ± 11	17.6 ± 1.9
$XylA_{XC}$-G15A-W147S	0.45 ± 0.01	70 ± 9	6.5 ± 0.9	1.24 ± 0.19	77 ± 10	16.0 ± 0.4

1003 **a** Mean ± S.D. of Michaelis-Menten non-linear regression fits of three independent replicates

1004

1005

1006 **Table 4. List of strains and plasmids used in this study**
1007

Strain or plasmid	Description	Reference
Strains		
E. coli DH5α	F^- φ80*lacZ*ΔM15 Δ(*lacZYA-argF*)*U169 recA1 endA1 hsdR17*(r_K^-, m_K^+) *deoR phoA supE44 thi*-1 *gyrA*96 *relA1* λ^-	[69]
C. glutamicum strains		
MB001	Prophage-free variant of the wild type ATCC 13032	[109]
MB001(DE3)	MB001 derivative with chromosomal integration of T7 RNA polymerase under control of P_{lacUV5}	[110]
Fru^{neg}	MB001 derivative with deletions of *ptsF* (cg2120) and *ptsG* (cg1537) and a *iolT1* (cg0223) promoter mutation preventing repression by IolR	This study
FXC evo	Fru^{neg} derivative with pPREx2-$xylA_{XC}$ evolved via adaptive laboratory evolution	This study
FAB evo	Fru^{neg} derivative with pPREx2-$xylA_{AB}$ evolved via adaptive laboratory evolution	This study
Fru^{neg}-IolT1^{G87S}	Fru^{neg} derivative with IolT1-G87S mutation	This study
Fru^{neg}-IolT1^{T351P}	Fru^{neg} derivative with IolT1-T351P mutation	This study
Fru^{neg}-Δ*glk*	Fru^{neg} derivative with *glk* (cg2399) deletion	This study
Fru^{negG}-Δ*glk*Δ*ppgK*	Fru^{neg}- Δ*glk* derivative with *ppgK* (cg2091) deletion	This study
Fru^{neg}-Δ*glk*Δ*ppgK*Δ*nanK*	Fru^{neg}-Δ*glk*Δ*ppgK* derivative with *nanK* (cg2932) deletion	This study
Glu^{neg}	Fru^{neg}-Δ*glk*Δ*ppgK*Δ*nanK* derivative with deletion of the gene clusters *iol1* (cg0196-cg0212) and *iol2* (cg3389-cg3393) and of *idhA3* (cg2313)	This study
Glu^{neg}-IolT1^{G87S}	Glu^{neg} derivative with IolT1-G87S mutation	This study
GXC evo	Glu^{neg}-IolT1^{G87S} derivative with pPREx2-$xylA_{XC}$-W147S evolved via adaptive laboratory evolution	This study
Glu^{neg}-IolT1^{G87S}-PtsS^{A129G}	Glu^{neg}-IolT1^{G87S} with PtsS-A129G mutation	This study
Suc^{neg}-IolT1^{G87S}	Glu^{neg}-IolT1^{G87S} with additional deletion of *ptsS* (cg2925)	This study
Plasmids		
pK19*mobsacB*	Kan^R, pK18 $oriV_{EC}$, *sacB*, *lacZα*, designed for genetic exchange in *C. glutamicum*	[71]
pK19*mobsacB*Δ*ptsF*	Kan^R, plasmid for *ptsF* (cg2120) deletion	This study
pK19*mobsacB*Δ*ptsG*	Kan^R, plasmid for *ptsG* (cg1537) deletion	This study
pK19*mobsacB*-P_{06}-*iolT1*	Kan^R, plasmid for mutation of *iolT1* (cg0223) promoter	[30]
pK19*mobsacB*-*iolT1*-G87S	Kan^R, plasmid for G87S mutation of *iolT1* (cg0223)	This study
pK19*mobsacB*-*iolT1*-T351P	Kan^R, plasmid for T351P mutation of *iolT1* (cg0223)	This study
pK19*mobsacB*Δ*glk*	Kan^R, plasmid for *glk* (cg2399) deletion	This study
pK19*mobsacB*Δ*ppgK*	Kan^R, plasmid for *ppgK* (cg2091) deletion	This study
pK19*mobsacB*Δ*nanK*	Kan^R, plasmid for *nanK* (cg2932) deletion	This study
pK19*mobsacB*Δ*iol1*	Kan^R, plasmid for *iol1* deletion covering cg0196-cg0212	[111]

pK19*mobsacB*Δ*iol2*	Kan^R, plasmid for *iol2* deletion covering cg3389-cg3393	[111]
pK19*mobsacB*Δ*idhA3*	Kan^R, plasmid for *idhA3* (cg2313) deletion	[23]
pK19*mobsacB*Δ*ptsS*	Kan^R, plasmid for *ptsS* (cg2925) deletion	This study
pK19*mobsacB*-*ptsS*-A129G	Kan^R, plasmid for A129G mutation in *ptsS* (cg2925)	This study
pPREx2	Kan^R, P_{tacI}, $lacI^q$, pBL1 $ori_{C.g.}$, pUC18 ColE1 $ori_{E.c.}$, consensus RBS (AAGGAG) for *C. glutamicum*	[112]
pPREx5	Kan^R, pPREx2 derivative with a His10-tag encoding sequence and a tobacco etch virus (TEV)-cleavage site	This study
pPREx2-$xylA_{AB}$	Kan^R, pPREx2 derivative containing D-glucose isomerase gene *xylA* of *Arthrobacter* strain N.R.R.L B3728 under the control of the *tac* promoter	This study
pPREx2-$xylA_{AG}$	Kan^R, pPREx2 derivative containing *xylA* of *Anoxybacillus gonensis* under the control of the *tac* promoter	This study
pPREx2-$xylA_{EC}$	Kan^R, pPREx2 derivative containing *xylA* of *E. coli* under the control of the *tac* promoter	This study
pPREx2-$xylA_{PE2}$	Kan^R, pPREx2 derivative containing *xylA* of *Piromyces* sp. E2 under the control of the tac promoter	This study
pPREx2-$xylA_{PR4}$	Kan^R, pPREx2 derivative containing *xylA* of *Paenibacillus* sp. R4 under the control of the *tac* promoter	This study
pPREx2-$xylA_{SM}$	Kan^R, pPREx2 derivative containing *xylA* of *Streptomyces murinus* under the control of the *tac* promoter	This study
pPREx2-$xylA_{XC}$	Kan^R, pPREx2 derivative containing *xylA* of *Xanthomonas campestris* under the control of the *tac* promoter	This study
pPREx2-$xylA_{AB}$-S2F	Kan^R, pPREx2-$xylA_{AB}$ derivative with S2F mutation in $xylA_{AB}$	This study
pPREx2(c_t)-$xylA_{AB}$	Kan^R, pPREx2-$xylA_{AB}$ derivative with cytosine to thymin mutation 20 bp upstream of the start codon	This study
pPREx2-$xylA_{XC}$-W147S	Kan^R, pPREx2-$xylA_{XC}$ derivative with W147S mutation in $xylA_{XC}$	This study
pPREx2-dae_{AG}	Kan^R. pPREx2 derivative with D-allulose 3-epimerase gene *dae* of *Arthrobacter globiformis*	This study
pPREx2-dae_{AT}	Kan^R, pPREx2 derivative with *dae* of *Agrobacterium tumefaciens*	This study
pPREx2-dte_{PC}	Kan^R, pPREx2 derivative with D-tagatose 3-epimerase gene *dte* of *Pseudomonas cichorii*	This study
pPREx2-$xylA_{XC}$-G15A-W147S	Kan^R. pPREx2-$xylA_{XC}$-W147S derivative with G15A mutation in $xylA_{XC}$	This study
pPREx2-$xylA_{XC}$-R24A-W147S	Kan^R. pPREx2-$xylA_{XC}$-W147S derivative with R24A mutation in $xylA_{XC}$	This study
pPREx2-$xylA_{XC}$-E124K-W147S	Kan^R. pPREx2-$xylA_{XC}$-W147S derivative with E124K mutation in $xylA_{XC}$	This study

pPREx2-*xylA*$_{XC}$-W147S-S286T	Kan^R. pPREx2-*xylA*$_{XC}$-W147S derivative with S286T mutation in *xylA*$_{XC}$	This study
pPREx2-*xylA*$_{XC}$-W147S-L299M	Kan^R. pPREx2-*xylA*$_{XC}$-W147S derivative with L299M mutation in *xylA*$_{XC}$	This study
pPREx2-*xylA*$_{XC}$-W147S-A421V	Kan^R. pPREx2-*xylA*$_{XC}$-W147S derivative with A421V mutation in *xylA*$_{XC}$	This study
pPREx2-*xylA*$_{XC}$-W147S-T427M	Kan^R. pPREx2-*xylA*$_{XC}$-W147S derivative with T427M mutation in *xylA*$_{XC}$	This study
pPREx2-*xylA*$_{XC}$-Strep	Kan^R, pPREx2-*xylA*$_{XC}$ derivative with Strep-tag fused to C-terminus of XylA$_{XC}$	This study
pPREx2-*xylA*$_{XC}$-W147S-Strep	Kan^R, pPREx2-*xylA*$_{XC}$-W147S derivative with Strep-tag fused to C-terminus of Xyl*A*$_{XC}$-W147S	This study
pPREx2-*xylA*$_{XC}$-G15A-W147S-Strep	Kan^R, pPREx2-*xylA*$_{XC}$-G15A-W147S derivative with Strep-tag fused to C-terminus of XylA$_{XC}$-G15A-W147S	This study
pPREx2-*xylA*$_{XC}$-*dae*$_{AT}$	Kan^R, pPREx2-*xylA*$_{XC}$ derivative with *dae* of *A. tumefaciens* downstream of *xylA*$_{XC}$	This study
pPREx2-*xylA*$_{XC}$-W147S-*dae*$_{AT}$	Kan^R, pPREx2-*xylA*$_{XC}$W147S derivative with *dae* of *A. tumefaciens* downstream of *xylA*$_{XC}$-W147S	This study
pPREx2-*xylA*$_{XC}$-G15A-W147S-*dae*$_{AT}$	Kan^R, pPREx2-*xylA*$_{XC}$-G15A-W147S derivative with *dae* of *A. tumefaciens* downstream of *xylA*$_{XC}$-G15A-W147S	This study
pPREx5-*xylA*$_{XC}$	Kan^R, pPREx5 derivative with *xylA* of *Xanthomonas campestris*	This study
pPREx5-*xlyA*$_{XC}$-W147S	Kan^R, pPREx5-*xylA*$_{XC}$ derivative with W147S mutation in *xylA*$_{XC}$	This study
pPREx5-*xylA*$_{XC}$-G15A-W147S	Kan^R, pPREx5-*xylA*$_{XC}$-W147S derivative with G15A mutation in *xylA*$_{XC}$	This study

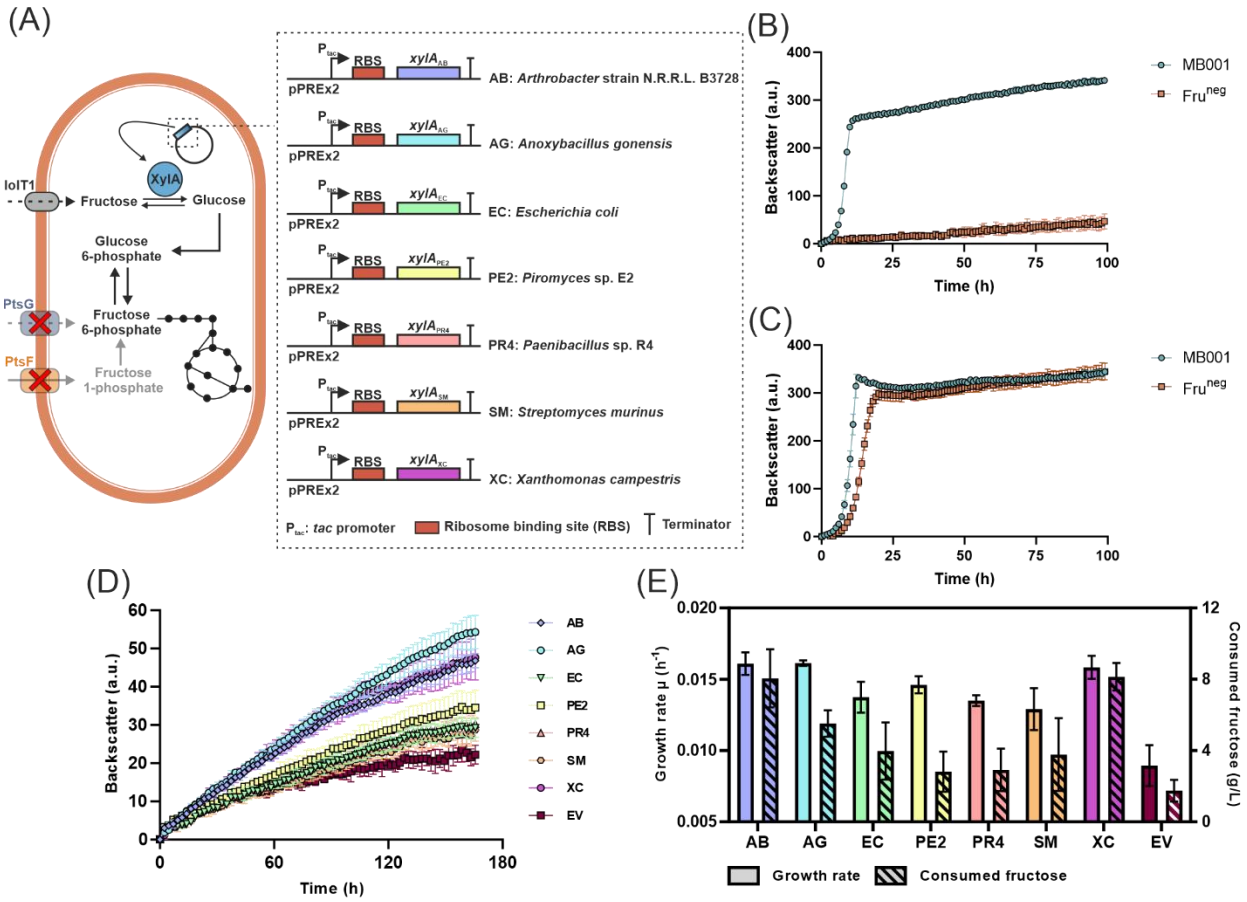

Figure 1. Growth-based selection system for the evaluation of D-glucose isomerase activity. (A) Coupling of D-glucose isomerase activity to the growth of the Fru^{neg} strain. The Fru^{neg} strain and its parental strain MB001 were cultivated in CGXII medium with 20 g/L D-fructose (B) or 20 g/L D-glucose (C) at 30°C and 1200 rpm for 100 h in a BioLector I microcultivation system. (D) Growth of Fru^{neg} transformed with either one of the seven *xylA* expression plasmids or the vector control pPREx2 (EV) in CGXII medium with 40 g/L D-fructose, 25 µg/mL kanamycin and 1 mM IPTG. The cultures were inoculated to an initial OD_{600} of 7.5. e Growth rates and consumed D-fructose titers of Fru^{neg} strains carrying different *xylA* variants shown in panel (d) after 160 h. All data points illustrate the mean ± S.D. from three biological replicates (n = 3).

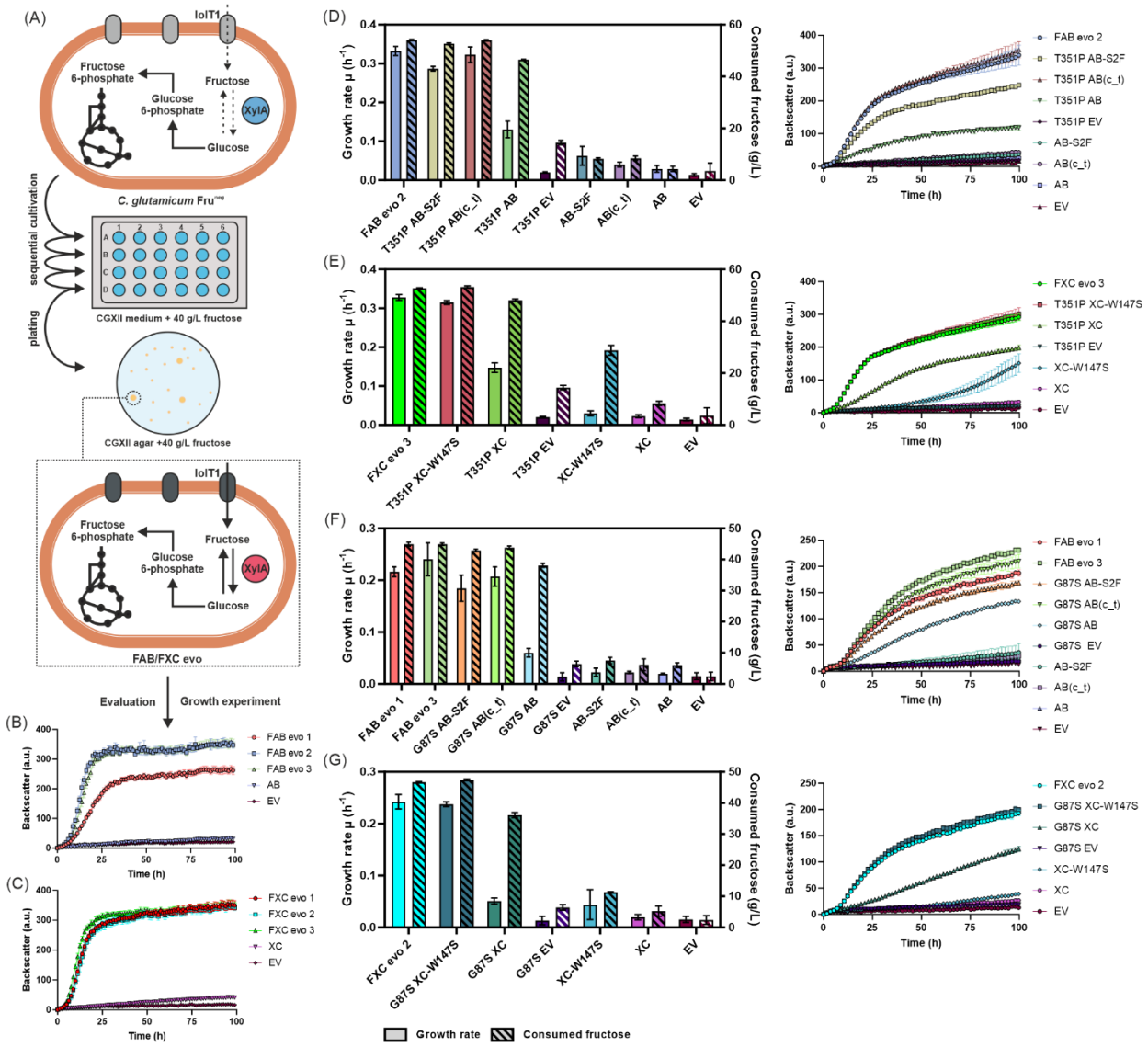

Figure 2. Evolution of Fru^{neg} strains with fast growth in D-fructose minimal medium. (A) Design of the adaptive laboratory evolution (ALE) experiment. Fru^{neg} strains carrying either pPREx2-*xylA*$_{AB}$ (AB) or pPREx2-*xylA*$_{XC}$ (XC) were sequentially cultivated in CGXII medium with 40 g/L D-fructose, 25 µg/mL kanamycin and 1 mM IPTG in 24-well plates at 30°C and 900 rpm. After the ALE was terminated each culture was diluted by a factor of 100,000 and plated on CGXII D-fructose agar plates to obtain single colonies. Comparatively large colonies were selected and used for a growth experiment in the same medium used for ALE (panels b and c). Each ALE was performed in biological triplicates. (B), (C) BioLector II growth experiments of the selected evolved AB and XC strains (FAB evo 1-3, FXC evo 1-3) in comparison to the unevolved parental strains (AB, XC) and the empty vector control (EV). (D), (E) Growth kinetics and D-fructose consumption of reverse engineered AB (D) and XC (E) strains containing *iolT1*-T351P (T351P) with pPREx2-*xylA*$_{AB}$-S2F (AB-S2F), pPREx2-*xylA*$_{AB}$(c_t) (AB(c_t)), pPREx2-*xylA*$_{XC}$-W147S (XC-W147S) or pPREx2 (EV). (F), (G) Growth kinetics and D-fructose consumption of reverse engineered AB (F) and XC (G) strains containing *iolT1*-G87S (G87S) with AB-S2F, AB(c_t), XC-W147S or EV. All growth experiments were conducted in CGXII medium with 40 g/L of D-fructose, 25 µg/mL kanamycin and 1 mM IPTG at 30°C and 1200 rpm for ~100 h either in BioLector I or II. The data shown represent the mean ± S.D. from three biological replicates (n = 3), except for XC (panel c) and EV (panel d-g) for which n = 2.

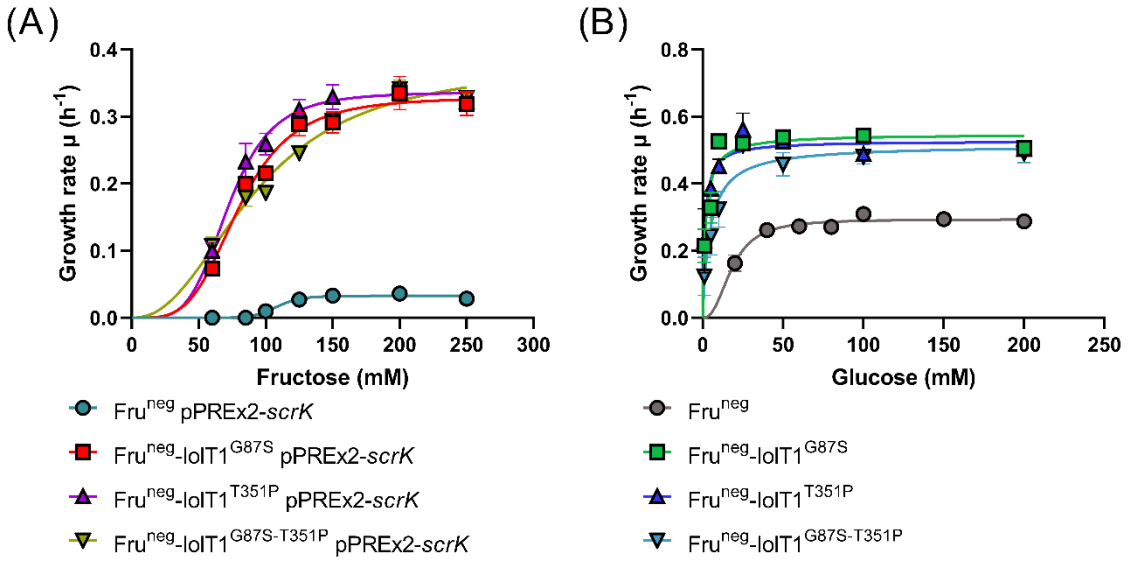

1040

1041 **Figure 3. Effects of the mutations G87S and T351P in IolT1 on growth with D-fructose and D-glucose as**
1042 **substrates.** (A) Growth experiments in D-fructose minimal medium were performed with Fru^{neg} strains containing the
1043 pPREx2-*scrK* plasmid, expressing fructokinase from *C. acetobutylicum*. The minimal medium was additionally
1044 supplemented with 1 mM IPTG and 25 µg/mL kanamycin. (B) Growth experiments in D-glucose minimal medium
1045 were performed with Fru^{neg} strains without a plasmid and minimal medium without IPTG and kanamycin. All
1046 experiments were performed in a BioLector XT at 30°C and 1200 rpm for 24-48 h. Inoculation was performed to an
1047 initial OD_{600} of 5. All data points given represent the mean ± S.D. of three biological replicates (n = 3). The data was
1048 fitted in GraphPad Prism using the default sigmoidal non-linear regression fit.

1049

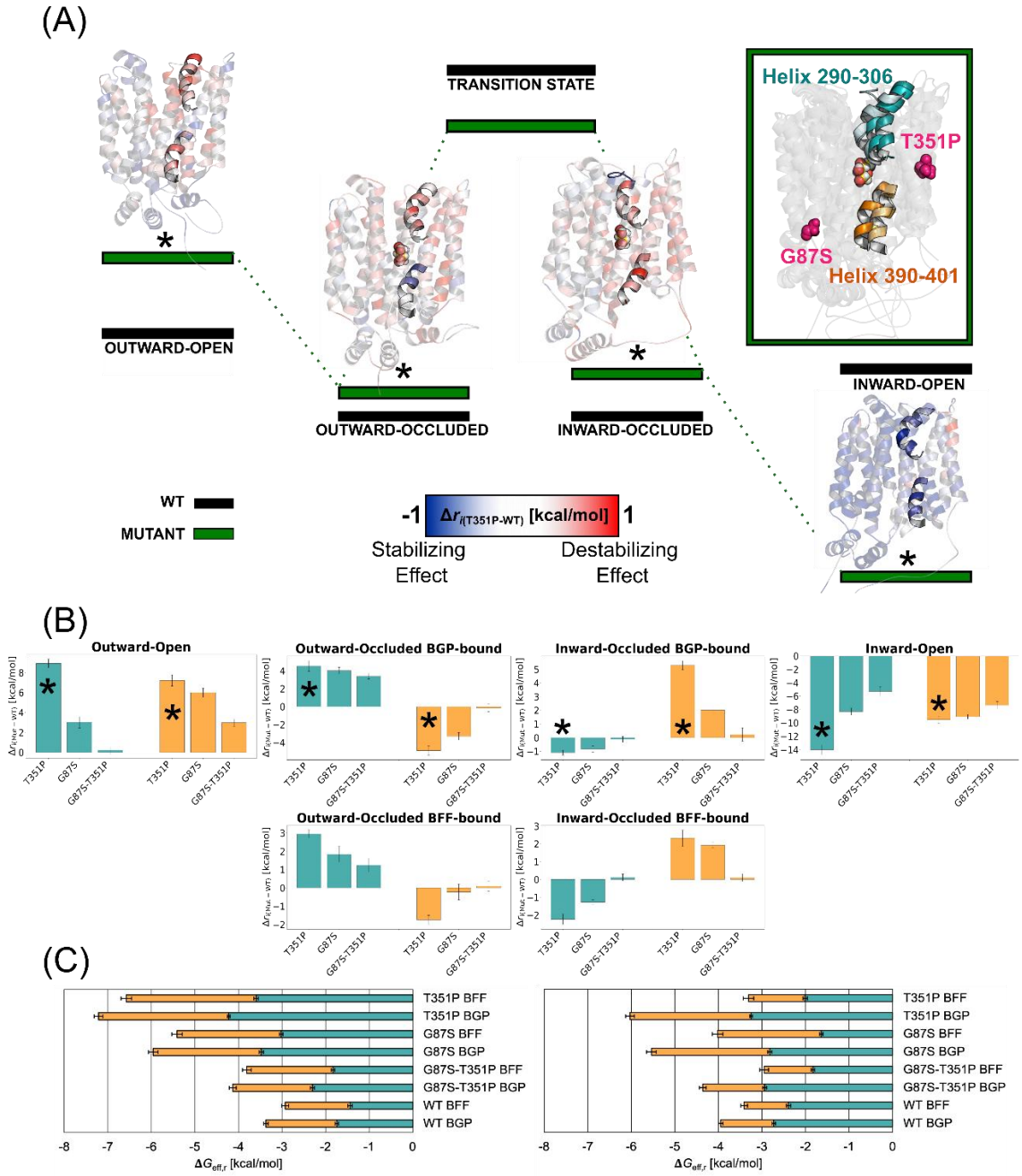

Figure 4. IolT1 mutations impacting D-glucose (β-D-glucopyranose, BGP) and D-fructose (β-D-fructofuranose, BFF) transport exert an allosteric effect on two helices critical to MSF transporter function. (A) IolT1-mediated transport is modeled using the induced transition fit (ITF) mechanism, where substrate binding supplies energy for conformational changes, resembling substrate destabilization in enzyme catalysis. The wild-type IolT1 energy profile (black bars, [42]) and T351P mutation effects (green bars) show how T351P destabilizes helices 290-306 and 390-401 in the outward-open state and stabilizes them in the inward-open state, facilitating substrate transport into the cell. The structural overlay of IolT1 highlights helix 290-306 (turquoise) and helix 390-401 (orange), with a gradient from outward- to inward-open states and the substrate (D-glucose), showing substitution sites G87S and T351P (magenta). (B) The difference $\Delta r_{r,(Mutant\text{-}WT)}$ (eq. 3, Supplemental Methods) across residues of helices 290-306 and 390-401 reveals that T351P has the greatest stabilizing effect, followed by G87S and G87S-T351P, correlating directly with cell growth trends. This stabilization effect is more pronounced with D-glucose than D-fructose. The asterisks (*) indicate the

values depicted in panel (A) as per-residue contributions. Error bars indicate the SEM. (C) $\Delta G_{\mathrm{eff,r}}$ sums per-residue contributions to effective binding energy for helices 290-306 and 390-401, in outward- (left) and inward-occluded (right) states, averaged from five replicas per variant. Error bars represent the propagated SEM and, thus, indicate the precision, not the accuracy, of the method. For all variants, D-glucose binding shows more favorable binding, reinforcing the trend from panel (B).

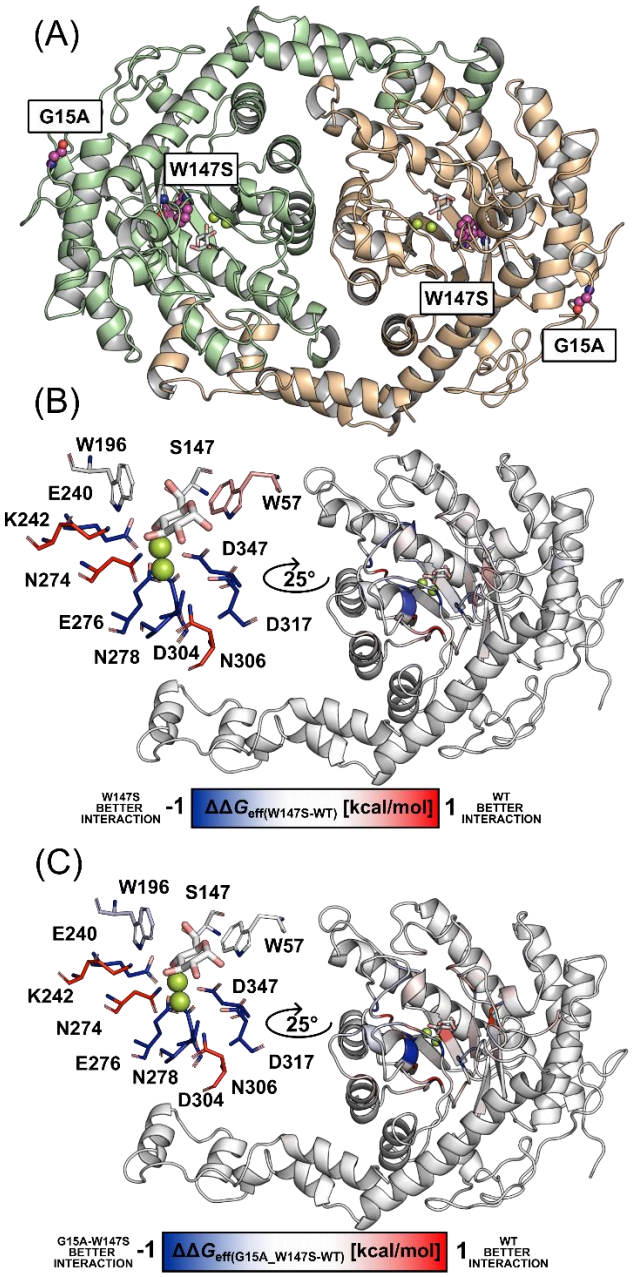

Figure 5. Mutation W147S impacts D-glucose (β-D-glucopyranose, BGP)-Mg^{2+} binding to the XylA homodimer. (A) The homodimeric structure of *X. campestris* $XylA_{XC}$ was predicted using AlphaFold3 [113]. The structure contains D-glucose-Mg^{2+} in the respective binding site of each monomer (green and orange ribbons). D-Glucose is depicted as white-salmon sticks and Mg^{2+} as lemon spheres. The mutation sites G15A and W147S are shown as purple spheres. (B) Differential per-residue effective binding energy ($\Delta\Delta G_{eff(W147S\text{-}WT)}$) mapped at the structural level. The energies were averaged across replicas. Larger changes in contributions to the effective binding energy occur near the D-glucose-Mg^{2+} binding site but encompass residues up to 15 Å away from position 147. Residues for which the largest differences were found are depicted as sticks and colored according to the color scale; red and blue colors indicate stronger binding by wild-type $XylA_{XC}$ and the W147S variant, respectively. **c** Differential per-residue effective binding energy ($\Delta\Delta G_{eff(G15A\text{-}W147S\text{-}WT)}$) mapped at the structural level. The energies were averaged across replicas. Residues for which the largest differences were found are depicted as sticks and colored according to the color scale; red and blue colors indicate stronger binding by wild-type $XylA_{XC}$ and the G15A-W147S variant, respectively.

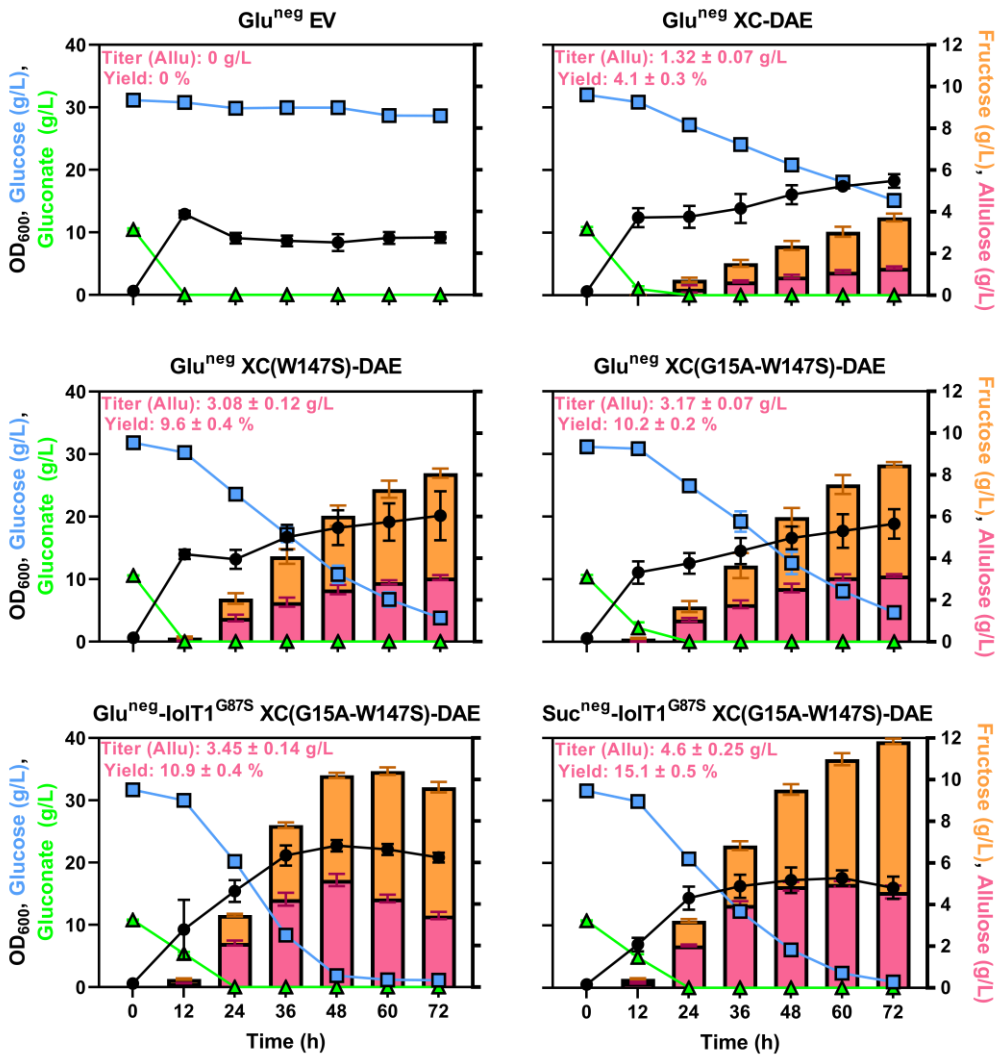

Figure 6. Production of D-allulose from D-glucose by *C. glutamicum* Glu^{neg} and Glu^{neg}-IolT1^{G87S}. The strains contained either pPREx2-*xylA*$_{XC}$-*dae*$_{AT}$ (XC-Dae$_{AT}$), pPREx2-*xylA*$_{XC}$-W147S-*dae*$_{AT}$ (XC-W147S-Dae$_{AT}$), pPREx2-*xylA*$_{XC}$-G15A-W147S-*dae*$_{AT}$ (XC-G15A-W147S-Dae$_{AT}$) or pPREx2 (EV). The experiment was conducted in CGXII medium with 10 g/L D-gluconate and 30 g/L D-glucose, 25 µg/mL kanamycin and 1 mM IPTG at 30°C and 130 rpm. Samples of the supernatant were taken every 12 h for a total time of 72 h. Growth was measured via OD_{600} and sugar concentrations were determined via HPLC. The data points represent average values with standard deviations of biological triplicates. The data shown represents the mean ± S.D. from three biological replicates (n = 3) or from two biological replicates (n = 2) for the 0 h sugar concentrations of Suc^{neg}-IolT1^{G87S}.